




The cooperative interplay among inflammation, necroptosis and YAP pathway contributes to the folate deficiency-induced liver cells enlargement

Wan-Yu Chi¹ · Tsun-Hsien Hsiao¹ · Gang-Hui Lee² · I-Hsiu Su² · Bing-Hung Chen^{3,4,5,6} · Ming-Jer Tang^{2,7} · Tzu-Fun Fu^{1,8} 

Received: 10 March 2022 / Revised: 10 June 2022 / Accepted: 13 June 2022 / Published online: 5 July 2022

© The Author(s), under exclusive licence to Springer Nature Switzerland AG 2022

Abstract

Change in cell size may bring in profound impact to cell function and survival, hence the integrity of the organs consisting of those cells. Nevertheless, how cell size is regulated remains incompletely understood. We used the fluorescent zebrafish transgenic line Tg-GGH/LR that displays inducible folate deficiency (FD) and hepatomegaly upon FD induction as in vivo model. We found that FD caused hepatocytes enlargement and increased liver stiffness, which could not be prevented by nucleotides supplementations. Both in vitro and in vivo studies indicated that RIPK3/MLKL-dependent necroptotic pathway and Hippo signaling interactively participated in this FD-induced hepatocytic enlargement in a dual chronological and cooperative manner. FD also induced hepatic inflammation, which convenes a dialog of positive feedback loop between necroptotic and Hippo pathways. The increased MMP13 expression in response to FD elevated TNF α level and further aggravated the hepatocyte enlargement. Meanwhile, F-actin was circumferentially re-allocated at the edge under cell membrane in response to FD. Our results substantiate the interplay among intracellular folate status, pathways regulation, inflammatory responses, actin cytoskeleton and cell volume control, which can be best observed with in vivo platform. Our data also support the use of this Tg-GGH/LR transgenic line for the mechanistical and therapeutic research for the pathologic conditions related to cell size alteration.

Keywords Cell size · Folate deficiency · YAP · Necroptotic pathways

✉ Tzu-Fun Fu
tffu@mail.ncku.edu.tw

¹ The Institute of Basic Medical Science, College of Medicine, National Cheng Kung University, Tainan, Taiwan

² International Center for Wound Repair and Regeneration, National Cheng Kung University, Tainan, Taiwan

³ Department of Biotechnology, Kaohsiung Medical University, Kaohsiung, Taiwan

⁴ Department of Medical Research, Kaohsiung Medical University Hospital, Kaohsiung, Taiwan

⁵ Center for Biomarkers and Biotech Drugs, Kaohsiung Medical University, Kaohsiung, Taiwan

⁶ Institute of Biomedical Sciences, National Sun Yat-Sen University, Kaohsiung, Taiwan

⁷ Department of Physiology, College of Medicine, National Cheng Kung University, Tainan, Taiwan

⁸ Department of Medical Laboratory Science and Biotechnology, College of Medicine, National Cheng Kung University, No. 1, University Rd., Tainan 701, Taiwan

Abbreviations

5-CH ₃ -THF	5-Methyltetrahydrofolate
5-CHO-THF	5-Formyltetrahydrofolate
AICART	Aminoimidazolecarboxamide ribonucleotide transformylase
DHFR	Dihydrofolate reductase
FA	Folic acid
FD	Folate deficiency
FDH	10-Formyltetrahydrofolate dehydrogenase
GART	Glycinamide ribonucleotide transformylase
Hx	Hypoxanthine
LEN	Lenalidomide
MAT	Methionine adenosyl transferase
MT	Methyltransferase
MTHFD	Methylenetetrahydrofolate dehydrogenase
MTHFR	Methylenetetrahydrofolate reductase
MTHFS	5,10-Methenyltetrahydrofolate synthetase
MTR	5-Methyltetrahydrofolate-homocysteine methyltransferase
NSA	Necrosulfonamide

OCM	One-carbon metabolism (OCM)
PRR16	Proline-rich protein 16
SAHH	S-adenosylhomocysteine hydrolase
SHMT	Serine hydroxymethyltransferase
TAZ	PDZ-binding motif
THF	Tetrahydrofolate
TS	Thymidylate synthase
VP	Verteporfin
YAP	Yes-associated protein
γ GH	γ -Glutamyl hydrolase

Introduction

The control of cell size is important for maintaining cell functionality and fitness. Change in cell volume or surface area will bring in profound impact to many basic cellular processes, such as nutrients distribution, intracellular transportation, the flux across cell membrane, energy generation and cell division [1]. Abnormal cell size also impairs transcription and translation [2, 3]. Therefore, alteration in cell size may affect cell survival and hence the integrity of the organs consisting of those cells. One of the most apparent consequences of cell size enlargement in vivo is organ growth. The size of an organ is determined mainly by the number and volume of the component cells. Cell enlargement has been recognized in several physiological processes, such as postnatal heart growth [4]. Altered cell size has been associated with pathological conditions, such as hypertrophic cardiomyopathy and renal hypertrophy [5]. While significant progress has been achieved in understanding the control of cell cycle and cell division in the past few decades, how cell size is regulated has hitherto is still mysterious.

Several pathways and mechanisms operating both in parallel and interactively have been proposed to modulate cell size [6]. The Hippo pathway is one of the best studied and highly conserved signaling pathways that regulate organ size, cell proliferation, apoptosis, differentiation, cell–cell contact and cell polarity. Yes-associated protein (YAP)/PDZ-binding motif (TAZ), is the major effector of the Hippo pathway. Overexpressing YAP in mice and zebrafish liver caused enlarged liver [7]. Contradictorily, mice with liver-specific knockout of YAP also displayed a mild liver enlargement and steatosis. Besides Hippo signaling, the mevalonate pathway participates in the synthesis of cholesterol and ubiquinone and has been found to control cell size through RAB11 GTPase and autophagy [8]. Overexpression of the proline-rich protein 16 (PRR16) gene product increased the size of hepatocyte [9]. Cell size homeostasis is also regulated by nutrients. *S. pombe* and *E. coli* grow larger in nutrients rich medium [10, 11]. One of the best-known examples correlating nutrition and cell volume is

folate deficiency (FD)-induced macrocytic anemia, a clinical manifestation displaying the phenotypic characteristics of enlarged red blood cells. However, the functional details for most of the mechanisms, including FD and cell size control, remain elusive.

Individual status of folate, a micronutrient participating in nucleotides biosynthesis and essential for cell proliferation and differentiation, has been known to affect cell size. In addition to genetic factors, environmental impacts, such as cell–cell contact, cell density and nutritional status, have also been shown to influence cell size. Folate, also known as vitamin B9, is composed of a pteridine ring, *p*-aminobenzoate and glutamyl moieties (Fig. 1a). The biologically active forms of folate are fully reduced tetrahydrofolate (THF), which is very unstable and easily lost in the process of cooking. Folate is the major one-carbon carrier with an one-carbon unit at the oxidation levels of formate, formaldehyde and methanol bound to THF at either the N-5 and/or N-10 positions, forming a large group of one-carbon adducts. In cells, folate exists as poly-glutamyl forms with five to eight glutamate residues attached to the γ -carbon of the first glutamate residue [12]. This polyglutamate tail helps retain the folate molecules inside the cells and increases the affinity of folate to folate enzymes. Dietary folate, mainly tri-glutamyl folate, needs to be converted to the monoglutamyl folate before up-take by intestine. Liver is the major organ for folate storage and metabolism since it contains the most abundant folate and almost all the enzymes involved in folate-mediated one-carbon metabolism (OCM). Folate participates in the biosynthesis of purine, pyrimidine, amino acids and neurotransmitter through OCM, hence is vital for rapidly growing tissues and proliferating cells, such as developing organ systems and cancer (Fig. 1b). Providing its one-carbon unit for the formation of S-adenosylmethionine (SAM), folate is also crucial to epigenetic control [13]. SAM is the primary methyl donor for most intracellular methylation reactions including DNA methylation. Reduced folate is a natural and strong antioxidant essential to maintaining intracellular oxidative stress and cell viability [12, 14, 15]. The multi-activity of folate endows this vitamin a modifiable environmental factor to prevent many important birth defects and associated diseases simply via dietary intervention. Meanwhile, as a reflection of the multiactivity possessed by folate, FD has been linked to various prevalent diseases, including neural tube defects, congenital heart diseases and Alzheimer's disease [16–18]. FD is one of the most frequently encountered clinical malnutrition. Nevertheless, how FD contributes to the etiology of these diseases, as well as cell size regulation, merit further investigation.

Studies with animal models of human diseases are indispensable, not only for pathomechanistic studies but also for the development of therapeutic strategies. This is especially true for studying the pathogenesis related

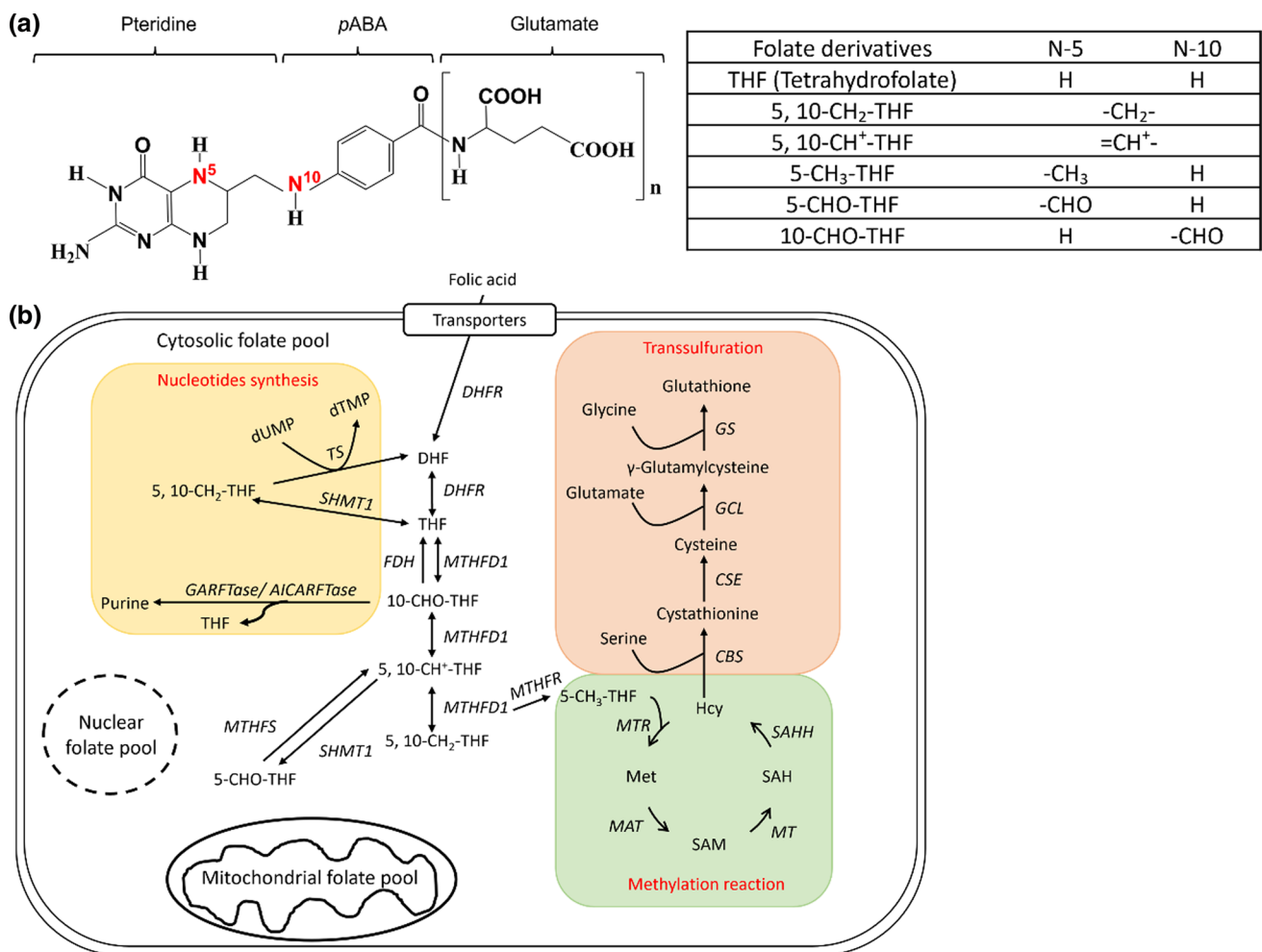


Fig. 1 Folate and folate-mediated one-carbon metabolism. **a** Folate is composed of a pteridine ring and a *p*-aminobenzoic acid with 5–8 γ -linked glutamate residues attached to the carboxyl group of benzene ring. The one-carbon unit is attached to N5- and/or N10-position of pteridine ring at the oxidation levels of formate, formaldehyde and methanol. **b** The one-carbon units carried by reduced folate participate in the biosynthesis of purines, thymidylate, amino acid and S-adenosylmethionine (SAM) in cytosolic, mitochondrial and nuclear folate pools. The folate enzyme γ -glutamylhydrolase (γ GH) converts polyglutamylfolates (folate-Glu_n) to monoglutamylfolates (folate-Glu₁) and facilitate intracellular folate exportation, leading to intra-

cellular folate deficiency (thickened circle and arrows in shadowed box). Enzyme abbreviations: *DHFR* dihydrofolate reductase, *MTHFD* methylenetetrahydrofolate dehydrogenase, *FDH* 10-formyltetrahydrofolate dehydrogenase, *GART* glycinamide ribonucleotide transferase, *AICART* aminoimidazolecarboxamide ribonucleotide transferase, *MTHFS* 5,10-methylenetetrahydrofolate synthetase, *SHMT* Serine hydroxymethyltransferase, *MTHFR* methylenetetrahydrofolate reductase, *TS* thymidylate synthase, *MTR* 5-methyltetrahydrofolate-homocysteine methyltransferase, *MAT* methionine adenosyl transferase, *MT* methyltransferase, *SAHH* S-adenosylhomocysteine hydrolase

to cell and organ size homeostasis since the complexity of cell–cell and cell–matrix interactions is better maintained in an in vivo system. Possessing both advantages of in vitro throughput and in vivo complexity, zebrafish offers an efficient platform for easy genetic manipulation and phenotypic endpoints examination [19]. In addition to the similarity in genetic composition and molecular operations between zebrafish and mammals, the convenience and economic in breeding of zebrafish has made this model animal ideal for complementing rodent for translational studies. Zebrafish has hitherto been effectively used in research fields of a wide-spectrum including molecular function,

diseases mechanism, developmental biology, toxicology and drug discovery. Zebrafish is especially prominent for studying in embryonic development for its transparent embryos/larvae and quick development. The study with zebrafish model on cell size control is just getting off the ground but promising since the same genetic pathways that govern cell size control in normal development have been shown to also affect pathological hypertrophy [20]. Therefore, detailed cell biological studies with zebrafish will be central to unveiling the complicate interactions between cell size, morphogenesis and disease etiology.

We found that FD caused liver cell enlargement both *in vitro* and *in vivo*, which cannot be prevented by nucleotides supplementation. Previously, we have established a zebrafish FD model, Tg(*lfabp*:mCherry/*hsp*:eGFP- γ GH), by over-expressing a fusion protein of γ -glutamylhydrolase (GGH), the enzyme hydrolyzing the polyglutamate tail of folate, with a fluorescent protein controlled by a heat-shock promoter (*hsp*) [12]. In contrast to polyglutamyl folate which will be retained intracellularly, monoglutamyl folate can cross cell membrane readily [21]. Therefore, the over-expressed GGH induced by heat-shock facilitates folate exportation, leading to diminished intracellular folate pools. The use of heat-shock promoter allows us to induce FD in an extent-, stage-and duration-controllable manner. The fusion of a fluorescent protein with GGH allows us to estimate the extent of GGH expression and FD. The expression of a fluorescent protein driven by a liver-specific promoter allows us to select transgenic fish without the need of heat-shock treatment and examine liver size in real-time without the need of sacrificing the experimental fish. With this double transgenic line, we found that zebrafish with FD displayed apparent hepatomegaly. Unlike the FD-induced macrocytic anemia, the liver enlargement observed in FD transgenic larvae could not be prevented by nucleotides supplementation. These observations were unexpected but suggested a mechanism other than disturbed nucleotides supply for the FD-induced liver cell enlargement. It also presents a potential platform for studying folate-related cell size regulation, prompting us to conduct the current study. Our results showed that it is mainly the interplay among the multiple pathways, including inflammation, YAP–TEAD signaling and necroptosis, instead of disturbed nucleotides supply, contributes to the etiology of enlarged liver cells.

Materials and methods

Material

5-methyl-THF were gift from Dr. Moser (Merck Eprova AG, Switzerland). 5-formyltetrahydrofolate was purchased from Schircks Laboratories (Bauma, Switzerland). Fetal bovine serum (FBS) and trypsin–EDTA were purchased from Invitrogen, Thermo Fisher Scientific Inc. (CA, USA). dNTP and dTTP were purchased from FocusBio (CA, USA). CAY10500 was purchased from Santa Cruz Biotechnology Inc. (DA, USA). Wortmannin, Nec-1s, and PF1052 were purchased from Abcam plc. (Cambridge, UK). Lenalidomide, GSK'872, necrosulfonamide, and Q-VD-Oph were purchased from BioVision, Inc. (SF, USA). Antibodies for immunostaining were purchased from either Santa Cruz Biotechnology Inc. (DA, USA) or Cell Signaling Technology Inc. (MA, USA). All other chemicals were purchased from

Sigma-Aldrich Chemical Co. (WI, USA). The HPLC gel filtration column AQUASIL C18 was purchased from Thermo Fisher Scientific Inc. (MA, USA).

Fish (*Danio rerio*) lines and maintenance

Zebrafish, including wild-type AB strain, Tg(*mpx*:eGFP) and Tg(*mpeg*:mCherry), were purchased from NTHU-NHRI Zebrafish Core Facility (supported by MOST 104-2321-B-001-045), Taiwan and bred and maintained at 28 °C in a 14-h light/10-h dark diurnal cycle following the standard procedure [22]. FD transgenic lines Tg(*lfabp*:mCherry/*hsp70*:eGFP- γ GH) (will be abbreviated as Tg-GGH/LR) and Tg(*lfabp*:eGFP/*hsp70*:mCherry- γ GH) (will be abbreviated as Tg-GGH/LG) were previously generated in our lab and regularly maintained at 25 °C [12].

Induction of folate deficiency

Adult fish and embryos were incubated in 38.5 °C for 8 h or 37.5 °C for an hour, respectively, following the protocols described in “Results”.

Compounds treatment

Most of the compounds and inhibitors were prepared as stocks in water or DMSO, added to embryo-containing E3 buffer and refreshed every other day unless otherwise mentioned. The concentrations for the inhibitors used were determined by referencing the literatures available and also tested for larval survival rate for optimization prior to applying the compounds to the experimental fish. The concentrations that allow for at least 90% survival rate will be chosen. The final concentrations used were: folic acid (FA) 1 mM, 5-formyltetrahydrofolate (5-CHO-THF) 1 mM, 5-methyltetrahydrofolate (5-CH₃-THF) 1 mM, wortmannin 20 nM, lenalidomide (LEN) 38.5 μ M, quercetin 2.5 μ M, dNTPs and dTTP 50 μ M, hypoxanthine 100 μ M, GdCl₃ 20 μ M, verteporfin (VP) 0.62 μ M [23], Nec-1s 20 μ M, GSK'872 15 μ M, necrosulfonamide (NSA) 5 μ M, MMP13 inhibitor 7.5 μ M, PF1052 0.1625 μ M [24], Q-VD-Oph 50 μ M [25], ATP 500 μ M, CAY10500 1 μ M.

Fluorescence determination of liver size

Larvae were anesthetized with 0.004% tricaine and imaged for larval lateral view under a fluorescence dissecting microscopy. The liver area was circled and quantified with the on-line software ImageJ, Threshold-Color plugin.

Folate content analysis

The total folate contents in cells and larvae extracts were measured with *Lactobacillus casei* assay with modifications [26]. In brief, cells (including cultured cells and dispersed cells prepared from larvae) were homogenized in extraction buffer (100 mM phosphate buffer pH 7.5, 2% ascorbic acid and 0.1% 2-mercaptoethanol) and centrifuged. Recombinant zebrafish γ -glutamyl hydrolase (γ GH) was added to the supernatant to convert the polyglutamyl folate to monoglutamyl folate. Aliquots of supernatant were added to *L. casei* suspension and incubated for 15 h at 37 °C before the optical density of the bacterial culture were recorded.

Intracellular folate content and composition were determined with an Aquasil C18 column on an HPLC system (Agilent 1100) as previously described [27]. The samples used here were prepared following the same procedure as aforementioned for the total folate measurement except that 30–45 embryos were used for each analysis.

Elastic modulus of zebrafish liver

Elastic modulus was measured using a JPK nanoWizard II atomic force microscope (JPK Instruments) as previously described with minor modifications [28]. Briefly, a tipless cantilever (CSC12, μ Mash) glued with 25 μ m (in diameter) polystyrene bead was prepared and calibrated with thermal noise method in protease inhibitor-contained PBS before measurement to reach a spring constant ranging within 0.2–0.6 N/m. For sample preparation, zebrafish liver was embedded in OCT at 4 °C overnight and dissected into 20 μ m sections at – 10 °C. Approximately 1–3 nN was applied to indent on the tissue section in PBS containing protease inhibitor, and force–distance curves were recorded. Young's modulus was calculated with the JPK's AFM software based on the Hertz model. The indentation depth was restricted to 1–2 μ m to avoid influence of the substrate.

Quantification for gene expression

For determining gene expression, RT-PCR, real-time PCR and Western blotting were performed as previously described [29]. The primers used in RT-PCR were: 5'-CGCATCTACAGCGGCACAGC-3' (forward) and 5'-GTTTCAGGACGCGGAACAGCC-3' (reverse) for zebrafish mmp13a; 5'-CGGTGCGGATCTTCAAAC-3' (forward) and 5'-TGTTTGGGAGTGACACG-3' (reverse) for zebrafish adam17b; 5'-AGACATCAAGGAGAAGCTGTG-3' (forward) and 5'-TCCAGACGGAGTATTTAC-3' (reverse) for zebrafish β -actin as internal control. The primers used in real-time PCR were: 5'-GGGACAAGTTGTTGGTGGT-3' (forward) and 5'-AAAGCGGCCACATCCTGT-3' (reverse) for zebrafish txn; 5'-GTCCACCGCAAATGCTTC-3' (forward) and 5'-ATT

GCCGTCACCTTCACC-3' (reverse) for zebrafish β -actin as internal control.

Cell culture

Cells were regularly maintained in Dulbecco's Modified Eagle medium (DMEM) containing 10% FBS and incubated in 5% CO₂ at 37 °C. For folate-deficient condition, cells were cultured in special α -Minimum Essential Medium, which was depleted for folate with exogenous addition of 5% charcoal-treated FBS, 0.003 g/L L-glycine, 0.03 g/L L-methionine, 0.042 g/L L-serine and 0.004 g/L pyridoxine.

Cell size and cell number analysis

Larvae were incubated in 2.5X trypsin–EDTA solution at room temperature for 20 min and manually dispersed. Cells (1×10^6 cells/ml), including both cultured cells and dispersed zebrafish larval cells, were thoroughly washed with PBS and subjected to flow cytometer (FACS CALIBUR, BD) for cell number and cell size determination following the manufacture's instruction. Cells were gated by FSC and SSC to eliminate debris and collect 10,000 cells to analyze cell size. Huh7, 293 T, and SK-N-SH cells (5×10^5 cells/dish) were seeded in 6-cm dishes and cultured in CTL or FD medium. Cells were harvested at 2-, 5- and 8-day post-seeding, stained with 0.2% trypan blue, and counted with a hemocytometer.

Immunostaining for cytoskeleton

Huh7 cells were fixed in 4% PFA/PBS for 15 min at room temperature and permeabilized with PBDBTx (PBS, 1% BSA, 1% DMSO, 0.5% Triton X-100) at least 2 h. Cells were incubated in mouse monoclonal anti-tubulin antibody 1:200 overnight at 4 °C. Huh7 cells were washed with PBS and incubated in goat anti-mouse IgG Alexa Fluor 594 (1:400) and Alexa Fluor 488 Phalloidin (1:200) for F-actin for 1 h at room temperature in the dark. Huh7 cells were stained with DAPI (1:2000) for 10 min and mounted with Fluoro-G mounting gel. The cytoskeleton of Huh7 cells was observed by FV3000 confocal laser scanning microscope.

Statistical analysis and reproducibility

Statistical significance was calculated with Student's t tests and Mann–Whitney nonparametric U test at 95% confidence intervals using the software GraphPad Prism 5 (GraphPad Software; San Diego, CA) with the error bars representing s.e.m..

Study approval

All use and experiments of adult and embryo were approved by the Institutional Animal Care and Use Committee, National Cheng Kung University, Tainan, Taiwan (IACUC Approval No. 106086).

Results

Hepatomegaly occurred to zebrafish larvae displaying FD

Our results showed that the livers of Tg-GGH/LR larvae were significantly enlarged when folate deficiency (FD) was induced at early embryonic development. The transgenic fish Tg-GGH/LR display red fluorescent liver and FD upon induction. To induce FD, four heat-shock protocols were designed and tested. Embryos/larvae were incubated at 37–39 °C for 1 h at the stages of either hepatic specification (protocol 1), liver differentiation (protocol 2) or post-liver development (protocol 3 and 4), and then evaluated for larval liver size at 11 days post fertilization (dpf) (Fig. 2a). The size of larval liver was observed and quantified by measuring the fluorescent area under a fluorescent dissecting microscope. Larval liver was apparently enlarged in those treated with protocol 2, 3 or 4, but showed no significant difference when FD was induced before 1 dpf (protocol 1) (Fig. 2b). An approximately 40% increase in size was found for the liver of the larvae treated with protocol 3 and 4. Examining the H&E stained cryo-sections prepared from 11 dpf larvae revealed apparently enlarged liver area with vacuoles in FD larvae (Fig. 2c). To minimize the interference on data interpretation raised from the impact to liver development and to allow for the maximal larval survival, protocol 3 was adopted for all the subsequent experiments. Measuring the intracellular total folate content of larvae at 7–11 dpf with microbiological assay revealed an approximately 40% decrease in the larvae treated with protocol 3, confirming FD status (Fig. 2d). Supplementing with either folic acid (FA), 5-formyltetrahydrofolate (5-CHO-THF) or 5-methyltetrahydrofolate (5-CH₃-THF) significantly alleviated liver hypertrophy, confirming the causal link between FD and enlarged liver (Fig. 2e). These results show that FD induced hepatomegaly in zebrafish larvae.

FD-induced hepatomegaly was not prevented by nucleotide supplementation

Organ size is mainly affected by the number and size of the cells constituting the organ. We observed no significant change in the size of liver of developing wild-type larvae from 7 to 11 dpf, indicating that hepatocytes might not

actively proliferate at these stages (Fig. 3a). Conversely, increasing liver size was found in FD larvae of the comparable stages. Folate is crucial to nucleotides formation and hence cell proliferation. Therefore, FD-induced enlarged liver is less likely caused by increasing the number of hepatocytes in FD larvae. Adding wortmannin, a potent inhibitor of cell proliferation, to embryos led to no further change in the liver size of both control and FD larvae (Fig. 3b). These results support the speculation that FD-induced hepatomegaly was not due to the impact to cell proliferation and cell numbers.

However, we could not exclude the possibility that FD might deplete intracellular nucleotide and lead to FD-induced pathology in a way other than impeding cell proliferation. Adding either deoxy-nucleotides or hypoxanthine, the nucleotides precursors, to larvae medium provided no appreciable rescuing effects (Fig. 3c). Further increase in liver size was even observed when dTTP and dNTP were added to embryo water. These results suggested that the hepatic nucleotides supply might not be significantly affected in FD larval liver. Examining the intracellular folate composition of FD larvae revealed significant decrease of both THF and 5-CH₃-THF in FD larvae (Fig. 3d and e). THF is the basic folate moiety of one-carbon carrier. 5-CH₃-THF provides the methyl group essential for the biosynthesis of SAM, the major methyl group donor for most intracellular methylation reaction. Contrarily, the level of 10-CHO-THF, the source of formyl group for purine production, in FD larvae was unaffected (Fig. 3f). Supplementing FD larvae with 5-CHO-THF restored THF and 5-CH₃-THF levels, whereas the content of 10-CHO-THF remained constant. These data are in line with our observations of the unproductive rescue with nucleotides supplementation for the hepatomegaly observed in FD larvae. These results suggested that cell proliferation and cell number were neither affected by FD nor contributed to the hepatomegaly observed in FD larvae.

Increased hepatic cell size and liver stiffness were found in vivo

The other determining factor on organ size is the size of the cells constituting the organ. For examining the size of hepatocytes, FD larvae with fluorescent liver were directly subjected to confocal microscopy imaging at 11 dpf. Quantification for the dimension of individual cells revealed significant enlargement of hepatocyte in FD larvae (Fig. 4a). Larval livers were also isolated, dispersed and analyzed with flow cytometry. The results showed that the size of hepatocytes isolated from FD larvae is approximately 1.4-fold larger than that of control larvae (Fig. 4b). In addition, the enlargement of hepatocytes was successfully prevented by 5-CHO-THF supplementation, confirming the causal link between FD and hepatocytic enlargement. Increased cell size

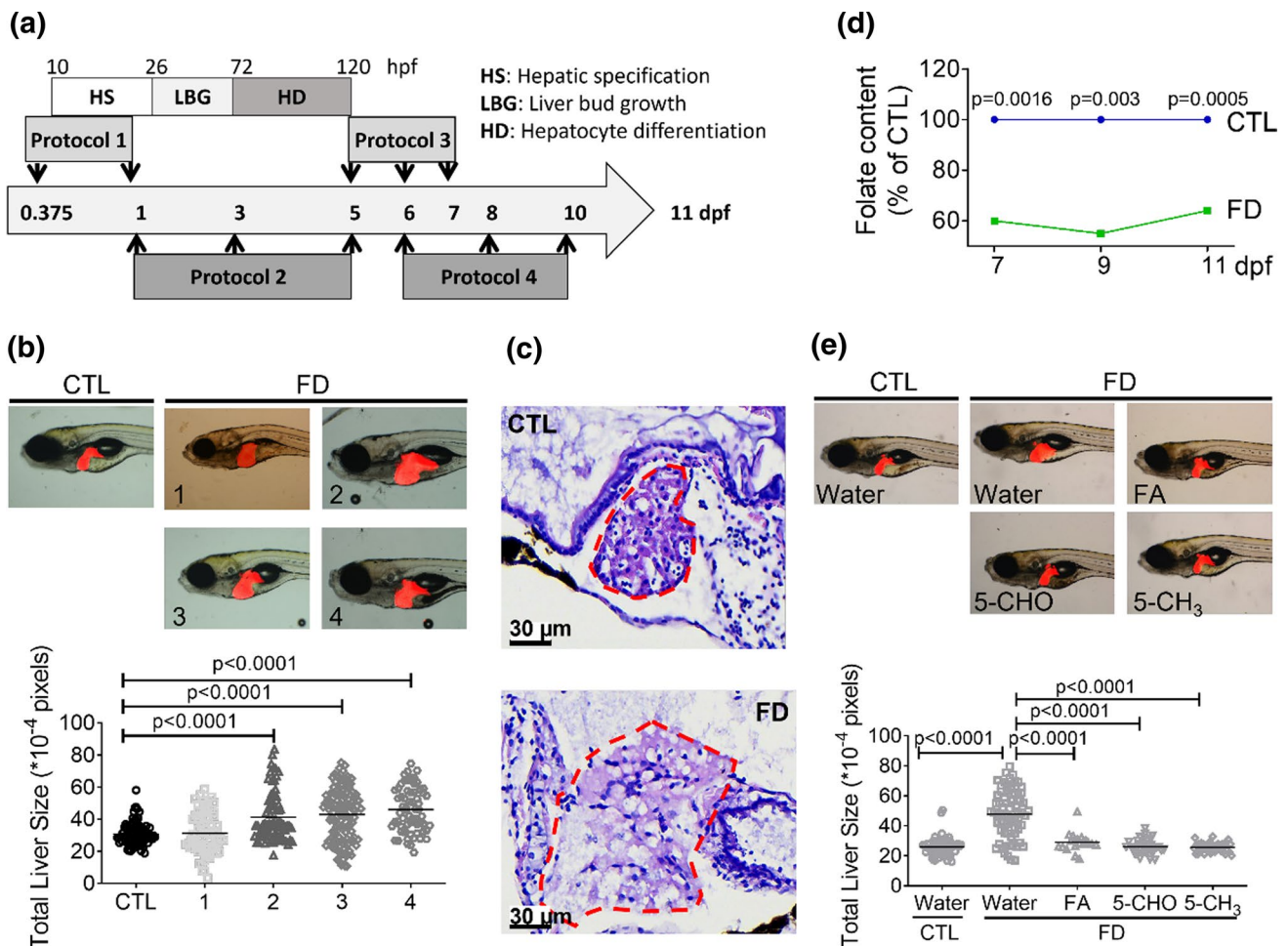


Fig. 2 Increased liver size was observed in zebrafish larvae displaying folate deficiency. The embryos/larvae generated from Tg-GGH/LR were induced for FD and examined for their liver size. **a** Embryos/larvae were heat-shocked repeatedly at 37–39 °C for 1 h at the indicated stages (arrows). Protocol 1, heat-shock twice at 9 and 24 hpf; protocol 2, three times at 1, 3 and 5 dpf; Protocol 3, three times at 5, 6, and 7 dpf; Protocol 4, three times at 6, 8 and 10 dpf. **b** Larvae treated with the four protocols were imaged under a fluorescence microscope at 11 dpf. Larval liver size was quantified by measuring the fluorescent area with the on-line software Image J. **c** Cryosections were prepared from larvae at 11 dpf and H&E stained.

Loosened tissue structure with apparent vacuoles was observed in the liver area (circled by red dashed line) of the larvae exposed to protocol 3, as compared to the untreated control. Scale bars=30 μm. **d** The larvae treated with protocol 3 were collected at 7, 9 and 11 dpf and examined for total folate content. **e** Larvae treated with protocol 3 were supplemented with folic acid (FA), 5-formyl-THF(5-CHO) or 5-methyl-THF(5-CH₃) starting from 7 dpf until 11 dpf. Larvae were imaged and quantified for liver size at 11 dpf. Statistical data are shown in mean ± SEM. CTL control (Tg-GGH/LR larvae without FD), FD folate deficiency

was also found in the hepatocytes of transgenic adult fish enduring FD, as compared to those of control, when the isolated liver was directly examined under confocal microscopy (Fig. 4c). These results showed that the size of hepatocytes was significantly increased in response to FD both in larvae and adult fish.

Liver stiffness was increased in FD zebrafish. Alteration in cell volume has been shown to change cell stiffness and cell fate [30]. To examine the potential impact of FD-induced hepatocytic enlargement to liver stiffness, fish liver from FD larvae and adult fish were isolated and examined for tissue elastic modulus. The results showed significant

increase in FD larval liver although no apparent difference was detected between the livers isolated from control and FD adult fish (Fig. 4d and e). These results showed that FD increased the size of hepatocytes and liver stiffness in vivo.

FD impeded cell proliferation, increased cell size and modulated cytoskeleton in cultured hepatocytes

For further examination with subsequent studies, three human cell lines: Huh7, 293 T and SK-N-SH, were cultivated in FD medium and recorded for cell growth and cell

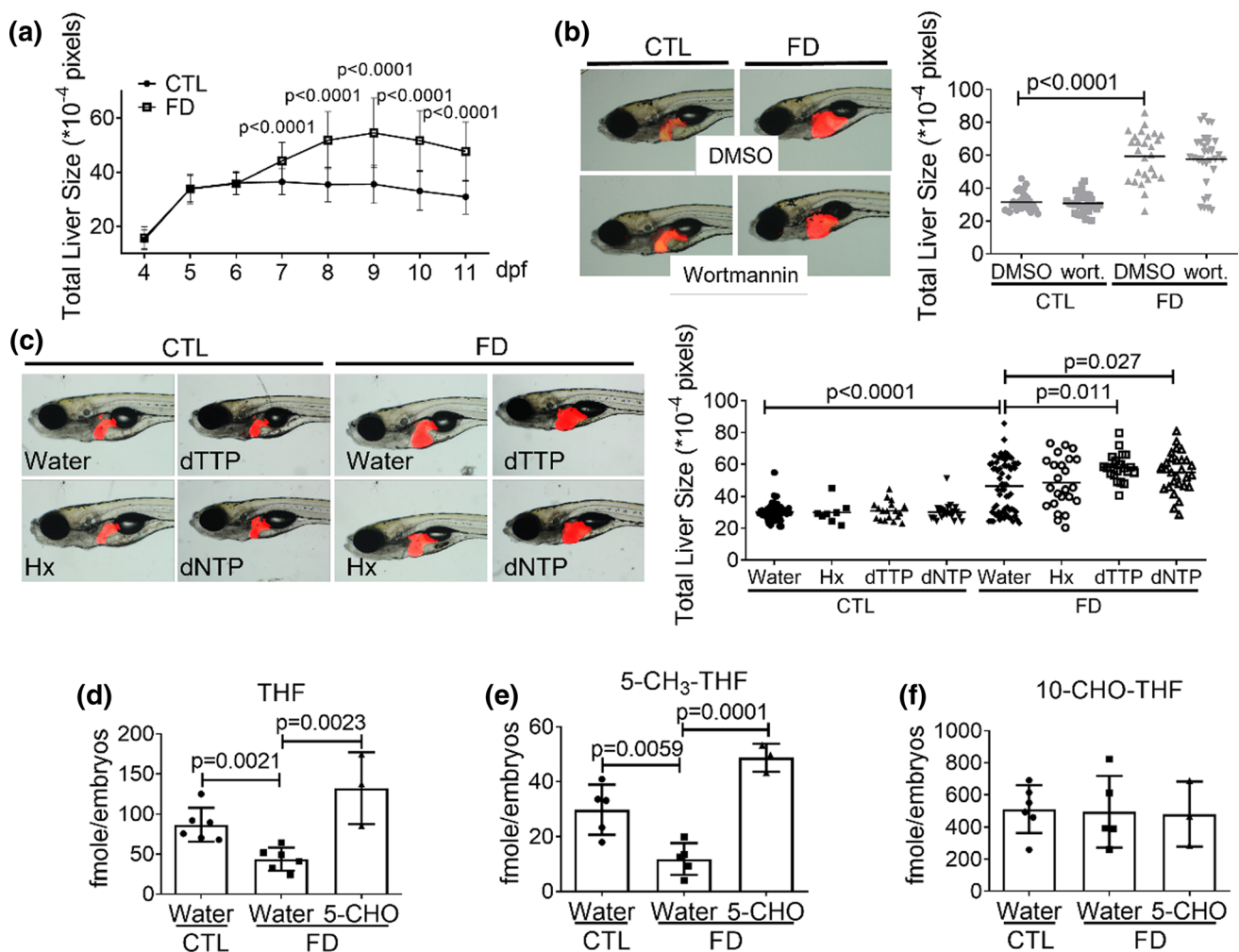


Fig. 3 FD-induced hepatomegaly was not prevented by nucleotide supplementation. Larval liver size was recorded daily by imaging the larvae under dissecting microscope and quantified with on-line software Image J (a). Larvae with/without exposure to wortmannin (20 nM) (b) and nucleotide supplement (c) starting from 7 dpf were evaluated for liver size. Liver size was quantified at 11 dpf using the on-line software Image J. **d–f** Larvae were collected at 11 dpf and

examined for folate derivatives contents. All the data presented are the averages of at least three independent trials with 10–40 larvae for each group. *Hx* hypoxanthine, *dTTP* deoxythymidine triphosphate, *dNTP* deoxynucleotide triphosphates. Statistical data are shown in mean \pm SEM. *CTL* control (Tg-GGH/LR larvae without FD), *FD* folate deficiency

cycle progression. Huh7 is an immortal human hepatoma cell line with a point mutation in the p53 gene [31]. 293 T is a highly transfectable derivative of human embryonic kidney 293 cells, and contains the SV40 T-antigen [32]. SK-N-SH is a neuroblastoma cell line that displays epithelial morphology with the potential of differentiating and adopting a neuronal phenotype [33]. Lack of appreciable cell growth was observed for all three cell lines with apparent inhibition starting from 2 days post seeding (dps) (Fig. 5a–c). Cell cycle arrest with significantly decreased cell number at G1 phase and accumulation of the polyploid cells also occurred (Fig. 5d–f). Unexpectedly, significant increase in cell size was observed for Huh7 cells and 293 T cells, but not for SK-N-SH (Fig. 5g). A 90%

decrease of intracellular total folate content was confirmed with microbiological assay in all three cell lines cultivated in FD medium for 8 days (Fig. 5h). The harvested Huh7 cells were also examined for individual folate content with HPLC. Significant decrease was found for both 5-methyltetrahydrofolate and 10-CHO-THF levels (Fig. 5i). THF was not detected in FD Huh7 cells. The results of immunostaining for cytoskeleton revealed apparent difference in F-actin which displayed perinuclear distribution in control Huh7 cells (Fig. 5j–m), but appeared to be circumferentially allocated at the edge under cell membrane when cells were cultivated in FD medium (Fig. 5n–q). These results showed that FD increased hepatic cell size and modulated the arrangement of intracellular F-actin.

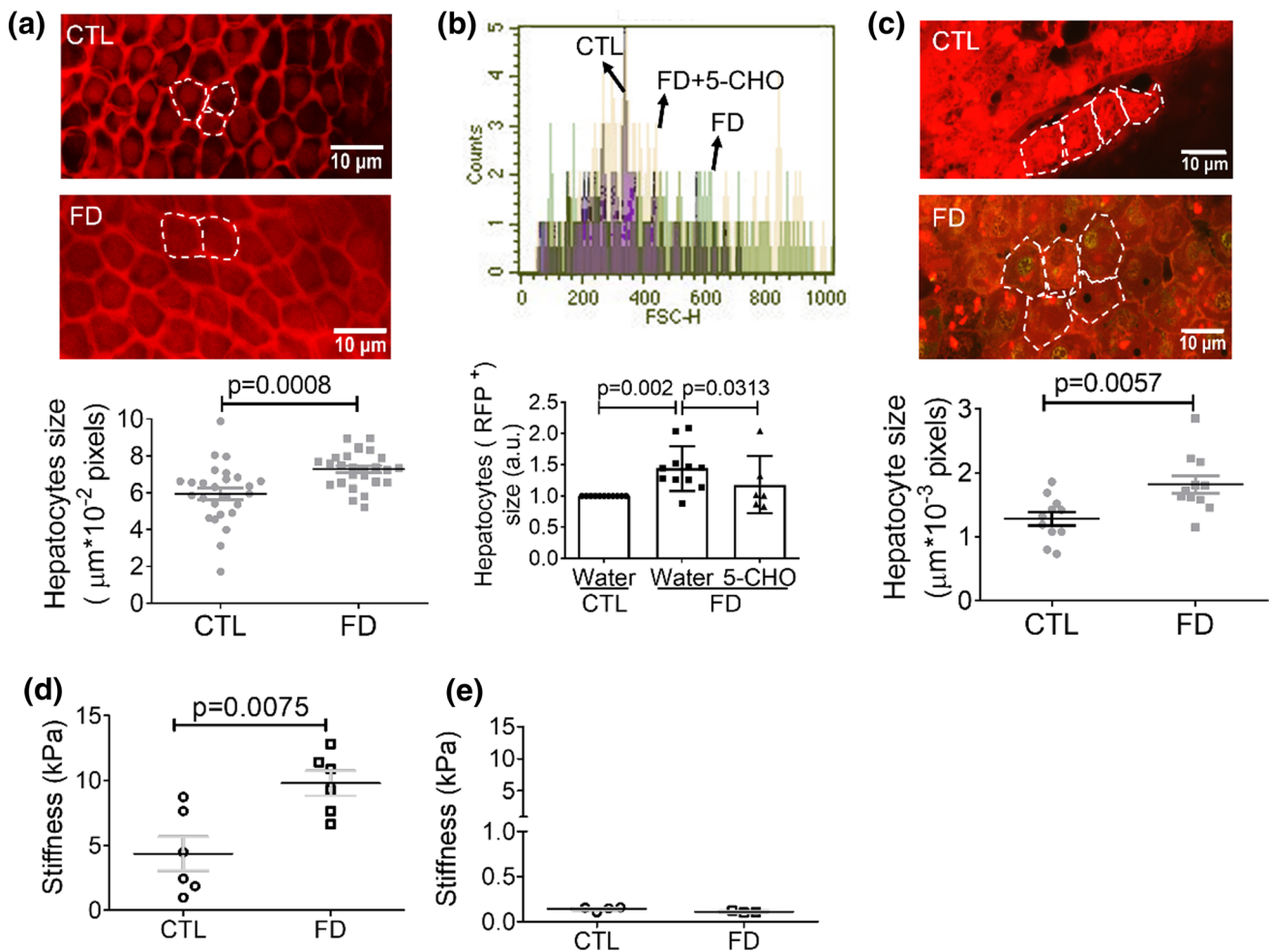


Fig. 4 Increased cell dimension was found in FD larval hepatocytes. **a** The hepatocytes of FD Tg-GGH/LR larvae were imaged under a fluorescence confocal microscope and quantified at 11 dpf. **b** FACS analysis on the dispersed red fluorescent liver cells prepared from FD larvae showed apparent increase in cell size, which was effectively prevented by the presence of 5-formyl-THF (5-CHO). Presented are the averaged results of at least six independent trials with each of the sample prepared from 20 to 30 larvae. The cell size obtained

with flow cytometry (FSC) was reported in arbitrary units (a.u.). **c** Confocal image analysis on the liver isolated from FD Tg-GGH/LR adult fish revealed increased dimension of hepatocytes. The fish livers isolated from larvae of 11 dpf (**d**) and adult fish (**e**) were examined for tissue elastic modulus. Significant increase in liver stiffness was detected in FD larval liver. CTL control (Tg-GGH/LR larvae without FD), FD folate deficiency. Statistical data are shown in mean \pm SEM. Scale bars = 10 μ m

Both RIPK3/MLKL(Necroptotic)-dependent pathway and Hippo pathway are interactively involved in FD-induced hepatomegaly

The possibility for the occurrence of apoptosis and necroptosis, the two main avenues of programmed cell death in response to restricted nutrition, was examined although organ hypertrophy is less likely caused by increased cell death. Adding Q-VD-Oph, an apoptosis inhibitor, did not prevent FD-induced liver hypertrophy (Fig. 6a). The results of TUNEL assay revealed no appreciable difference for the apoptotic signal between the livers of control and FD larvae (Fig. 6b). Curiously, adding NSA, a potent inhibitor of necroptosis, alleviated the hepatomegaly observed in FD

larvae although trypan blue staining revealed no apparent necrotic/necroptotic death in FD larvae (Fig. 6a and data not shown). These results suggested that the MLKL-dependent (necroptotic) pathway was activated but did not cause significant cell death. In addition, the activation of necroptotic pathway, but not apoptosis, likely played a role in the enlargement of FD larval liver. These results are unexpected but conceivable since increased cell size has been known to be an early morphological characteristic of necroptosis [34].

Further examination on the activation of necroptotic pathway revealed significant increase of phosphorylated MLKL in Huh7 cells cultivated in FD medium (Fig. 7a). The phosphorylation of MLKL, a key component in necroptotic pathway, is crucial for initiating necroptosis.

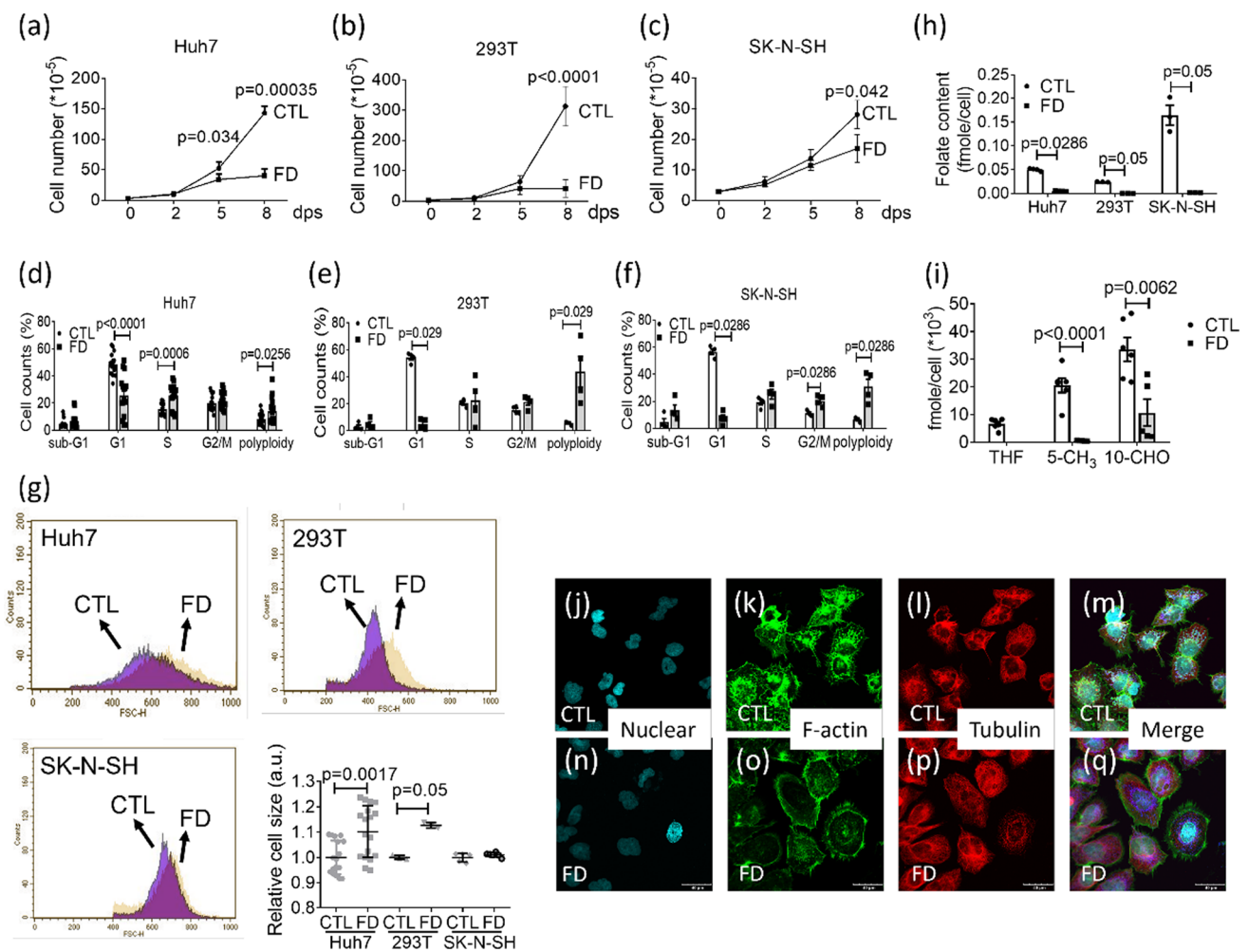


Fig. 5 Cell enlargement and altered F-actin distribution in FD liver cells. Cells grown in FD medium were recorded for cell number daily (a–c). The numbers shown on the Y-axis equate to (the actual cell numbers) times the multiplier, 10^{-5} , shown in the parentheses of the Y-axis title. Cells were also harvested after cultivating for 8 days and examined for cell cycle (d–f), cell size (g) and total folate content

(h). The cell size obtained with flow cytometry (FSC) was reported in arbitrary units (a.u.). Huh7 cells cultured in regular (CTL) or folate-deficient α -MEM (FD) were further analyzed with HPLC for individual folate derivatives (i) and immuno-stained for cytoskeleton distribution (j–q). Scale bars=40 μm . Statistical data are shown in mean \pm SEM

RIPKs are the major components essential for forming MLKL complex that ruptures plasma membrane. Adding RIPK1 and RIPK3 inhibitors to embryo water also effectively alleviated FD-induced liver hypertrophy (Fig. 7b). In addition, the presence of inhibitors for necroptosis and RIPK3, but not RIPK1, effectively ameliorated the FD-induced enlargement of larval hepatocytes (Fig. 7c). ATP depletion is one of the biochemical hallmarks of necroptosis, which also distinguishes necroptosis from apoptosis [35]. Supplementing with ATP alleviated liver hypertrophy, further supporting the involvement of necroptotic pathway in FD-induced hepatomegaly (Fig. 7d). These results suggest that the activation of RIPK3/MLKL-dependent necroptotic pathway contributed to FD-induced hepatomegaly.

Increased protein levels for both total YAP and pYAP^{s127} but with decreased ratio of pYAP^{s127}/YAP were found in FD Huh7 cells (Fig. 8a). YAP is the effector of Hippo signaling cascade, a master regulator of organ size and tissue growth. De-phosphorylation of YAP at serine127 (YAP^{s127}) is essential for the intra-nuclear localization of YAP and the activation of subsequent transcription [36]. In addition, a more than twofold increase in *txn* transcript was observed for FD adult fish liver (Fig. 8b). *Txn* is one of the down-stream genes regulated by nuclear-localized YAP/TAZ–TEAD complex. Increased *txn* expression was also found for FD whole larvae and the liver isolated from FD larvae. We would like to note that supplementing with 5-CHO-THF did not lower the expression of *txn* when the extracts prepared from whole larvae were used for examination (Fig. 8c). Considering the

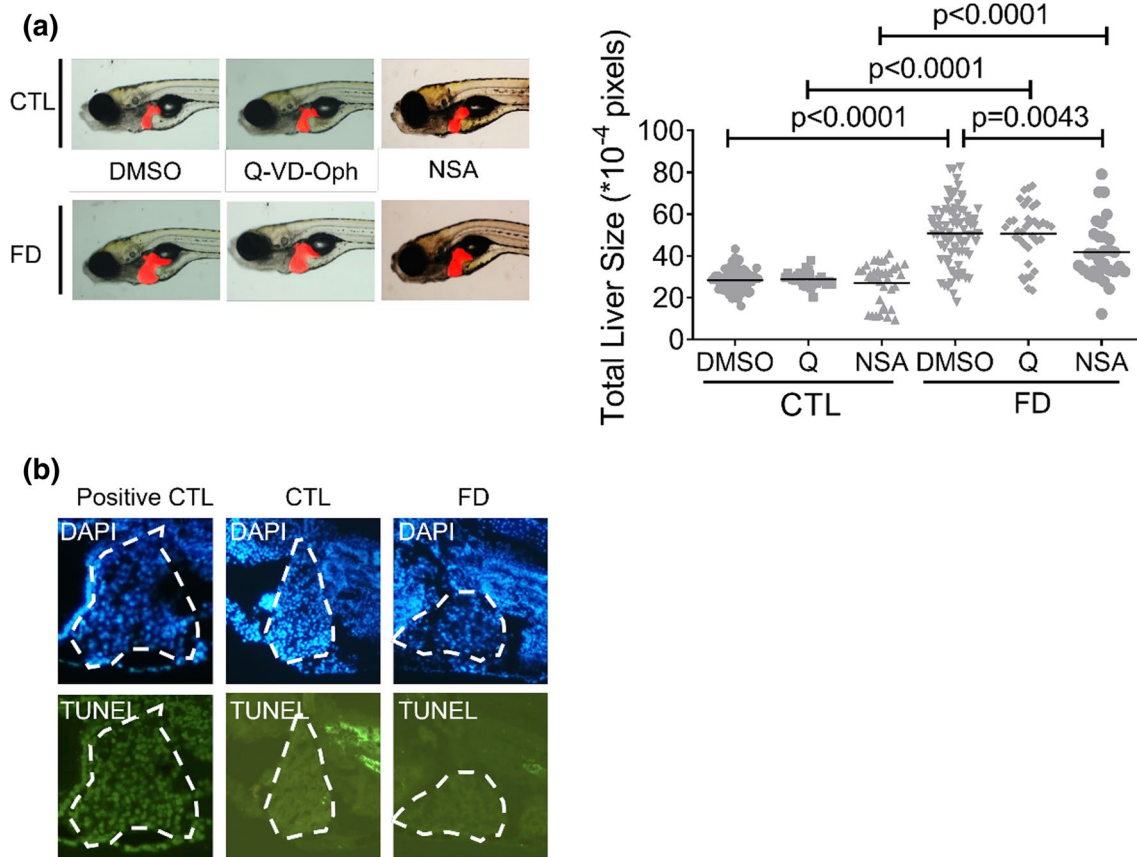


Fig. 6 Inhibiting necroptosis alleviated FD-induced liver hypertrophy. **a** Larvae exposed to apoptosis inhibitor Q-VD-Oph (Q, 50 μ M) or necroptosis inhibitor NSA (5 μ M) starting from 7 dpf were imaged and quantified for liver size at 11 dpf. **b** The hepatic cryo-sections prepared from the larvae at 11 dpf were subjected to TUNEL assay

for apoptotic cells. No apparent apoptotic signal was found in the liver (circled) of both control and FD larvae, as compared to positive control (sample pretreated with DNase). Statistical data are shown in mean \pm SEM. CTL control (Tg-GGH/LR larvae without FD), FD folate deficiency

tissue specificity of folate-mediated OCM, these results are not unexpected since the obtained results would reflect the combined effect from all larval tissues/organs. Contrarily, the decrease of *txn* expression became significant, in response to 5-CHO-THF supplementation, when isolated larval livers were used as samples (Fig. 8d). Verteporfin is a Hippo pathway inhibitor functioning by disrupting YAP/TAZ-TEAD interactions. Adding verteporfin to embryo water ameliorated both liver hypertrophy and FD-induced hepatocytes enlargement (Fig. 8e and f). In addition, knocking down YAP expression by transfecting with siYAP has significantly decreased YAP protein levels and prevented the FD-induced cell size enlargement in Huh7 cells (Fig. 8g and h). These results support the causal link between FD-induced hepatomegaly and Hippo pathway activation, as well as the tissue-specific response to altered folate status.

We also found that adding verteporfin to Huh7 cells cultivated in FD medium decreased MLKL phosphorylation, indicating the participation of YAP signaling in the FD-induced activation of necroptotic pathway (Fig. 9a). No

apparent change was observed in the pMLKL/MLKL ratio of FD Huh7 cells when TNF α inhibitor LEN was added to culture medium for rescue. These results suggest that TNF α might not contribute significantly to the activation of necroptotic pathway in FD Huh7 cells in vitro. Nevertheless, adding both verteporfin and NSA simultaneously to embryo water did not provide additive rescuing effect for the size of either FD larval liver or cultured Huh7 cells (Fig. 9b and c). These data suggested that FD modulated both Hippo pathway and necroptotic signaling, which contributed to the FD-induced hepatomegaly. In addition, these two pathways may function interactively via the same route likely in an upstream–downstream cooperative manner.

Inflammation and TNF α participated in FD-induced hepatomegaly

The discretely reported interplays among inflammation, necroptosis and Hippo pathway prompted us to examine whether inflammation also played a role in FD-induced

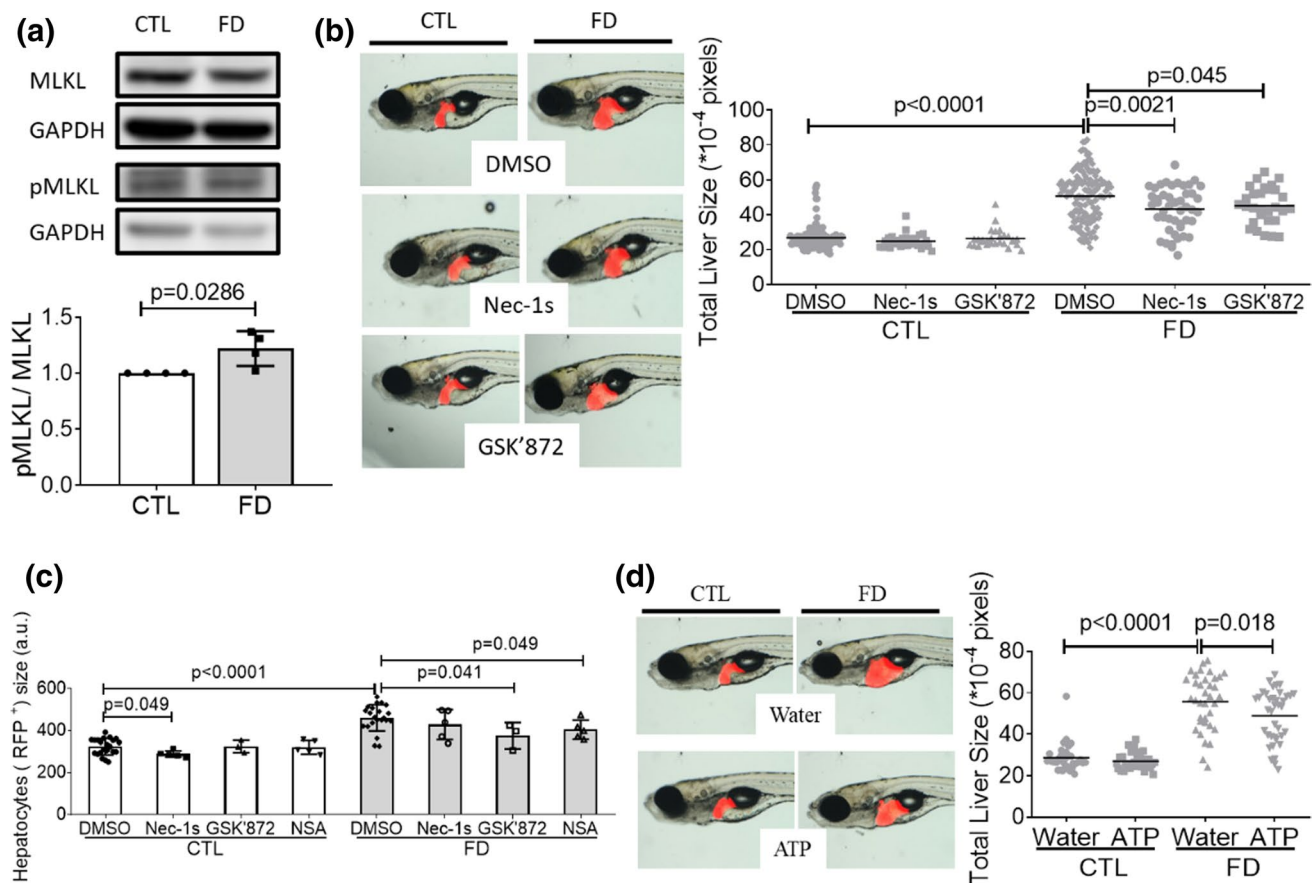


Fig. 7 Activated necroptotic pathway was involved in FD-induced liver hypertrophy. **a** Cell lysates prepared from Huh7 cells cultivated in regular (CTL) or FD medium were analyzed with Western blotting for MLKL phosphorylation and quantified with densitometry. **b** The liver size of larvae exposed to Nec-1s (20 μ M, RIPK1 inhibitor) or GSK'872 (15 μ M, RIPK3 inhibitor) starting from 7 dpf were imaged and quantified at 11 dpf. The presence of RIPKs inhibitors significantly improved liver hypertrophy. **c** FACS analysis on the dispersed red fluorescent liver cells prepared from 11 dpf larvae exposed

to necroptosis and RIPKs inhibitors showed significant decrease for the enlarged cell size. Shown here are the averaged results of at least five independent trials with each sample prepared from 20 to 30 larvae. The cell size obtained with flow cytometry (FSC) was reported in arbitrary units (a.u.). **d** The liver sizes of larvae grown in embryo water with/without additional ATP were imaged and quantified. CTL control (Tg-GGH/LR larvae without FD or Huh7 cells cultured in regular α -MEM), FD folate deficiency

hepatomegaly [37–40]. The embryos generated from the triple transgenic lines Tg(*lfabp*:mCherry/*hsp70*:eGFP- γ GH/*mpx*:eGFP) and Tg(*lfabp*:eGFP/*hsp70*:mCherry- γ GH/*mpeg1*:mCherry) were used to assess the involvement of neutrophils and macrophages, respectively. Tg(*lfabp*:mCherry/*hsp70*:eGFP- γ GH/*mpx*:eGFP) display red fluorescent liver, green fluorescent neutrophils and FD upon induction. By the same token, Tg(*lfabp*:eGFP/*hsp70*:mCherry- γ GH/*mpeg1*:mCherry) display green fluorescent liver, red fluorescent macrophages and FD upon heat shock. Apparent infiltration of both neutrophils and macrophages were found in larval liver area of FD larvae in a time-dependent manner (Fig. 10a and b). Adding neutrophil inhibitor PF1052 to embryo water decreased the number of neutrophils in FD larval liver area but did not prevent hepatomegaly (Fig. 10c and d). On the

other hand, adding quercetin and GdCl₃ to embryo water significantly rescued FD larvae from hepatomegaly (Fig. 10e). Both quercetin and GdCl₃ are macrophages inhibitors. These results suggested that the activation of macrophages might play a role in FD-induced hepatomegaly. Significant increase of Mpeg protein, the macrophage specific marker, was found in FD adult fish liver, confirming the activation of macrophages (Fig. 10f). The presence of quercetin and GdCl₃ has alleviated the increased Mpeg expression in response to FD when the whole larvae extracts were subjected to Western blotting (data not shown). Analysis on the size of the hepatocytes isolated from GdCl₃-treated FD larvae also showed significant decrease in comparison to those without GdCl₃ exposure (Fig. 10g). More intriguingly, inhibiting YAP signaling and necroptotic pathway also alleviated FD-induced macrophage infiltration (Fig. 10h). These

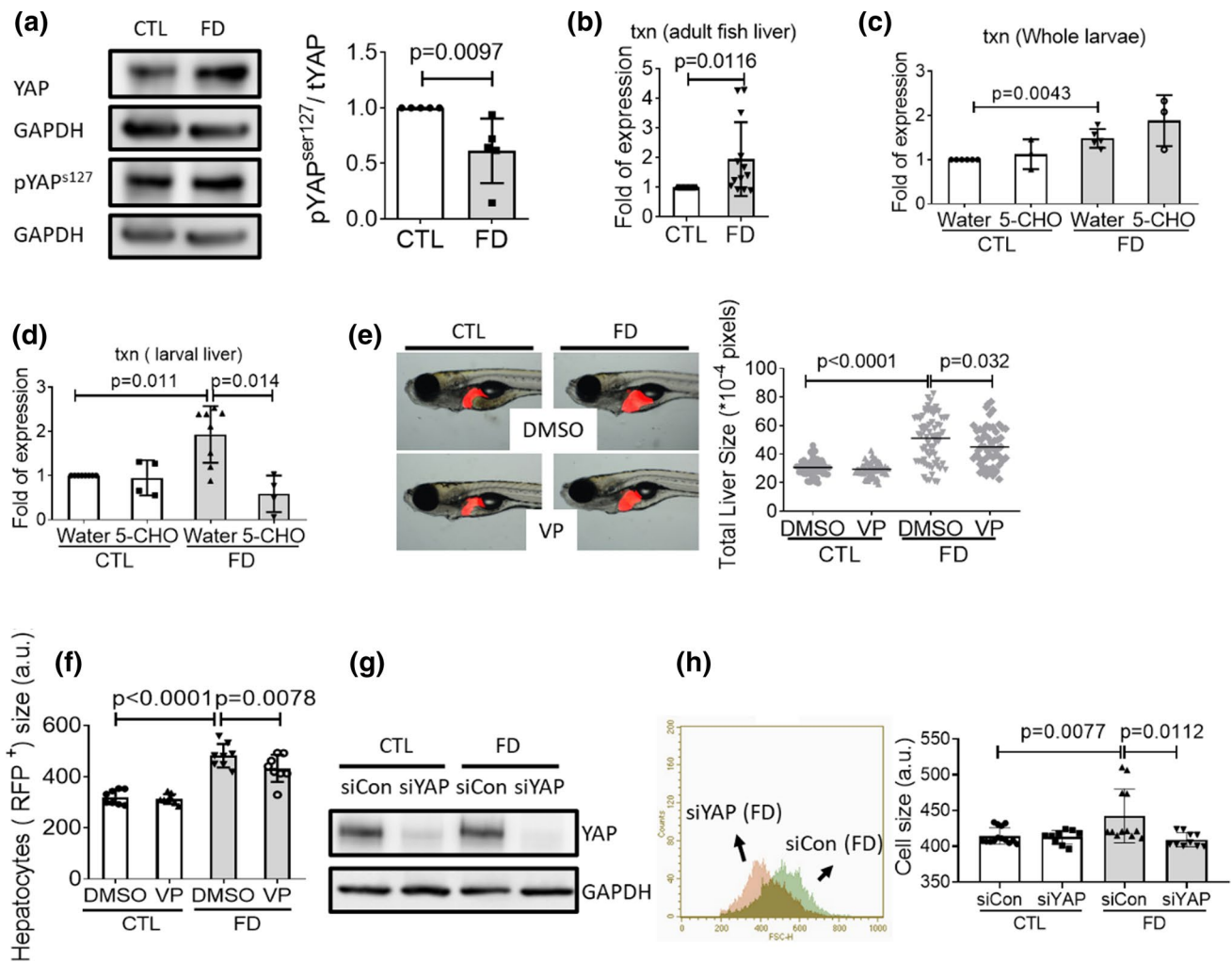


Fig. 8 Activation of Hippo pathway contributed to FD-induced hepatomegaly. **a** Cell lysates prepared from Huh7 cells cultivated in regular (CTL) or FD medium were analyzed with Western blotting for the level of total YAP and pYAP^{S127} and quantified with densitometry. The results of Real-time PCR revealed increased txn transcripts in the extracts prepared from FD adult fish liver (**b**), FD whole larvae of 11 dpf (**c**) and FD larval liver (**d**). **e** The liver size of larvae exposed to verteporfin (VP, 0.62 μ M) starting from 7 dpf were imaged and quantified at 11 dpf. **f** FACS analysis on the dispersed red fluorescent liver cells prepared from 11 dpf larvae exposed to VP showed significant decrease for the enlarged cell size. Shown here are the averaged results of at least eight independent trials with each sample prepared from 20 to 30 larvae. Huh7 cells were cultivated in regular (CTL) or FD medium and transfected with siCon or siYAP at 4-day post-seeding (dps). Cells were harvested and subjected to Western blotting (**g**) and flow cytometry (**h**) at 7 dps. The cell size obtained with flow cytometry (FSC) was reported in arbitrary units (a.u.). 5-CHO 5-formyltetrahydrofolate. Statistical results are represented in the mean \pm SEM. CTL control (Tg-GGH/LR larvae without FD or Huh7 cells cultured in regular α -MEM), FD folate deficiency

results suggested that FD induced hepatic inflammation in larval liver, which contributed to the FD-induced hepatocytes enlargement and hepatomegaly.

Our results also showed that the activity of tumor necrosis factor α (TNF α) was involved in FD-induced hepatomegaly. TNF α is a key pro-inflammatory cytokine secreted primarily by immune cells, especially macrophages. We found that the level of TNF α protein was significantly increased in the extracts prepared from liver, but not eyes and whole larvae at 11 dpf (Fig. 11a). Increased TNF α was also detected in the used culture medium when Huh7 cells were cultivated under FD

condition for 8 days (Fig. 11b). Adding TNF α directly into medium increased the cell size and decreased intracellular pYAP^{S127}/tYAP ratio of cultured Huh7 cells (Fig. 11c and d). In addition, adding TNF α inhibitors lenalidomide (LEN) and CAY10500 (CAY) to embryo water significantly alleviated the hypertrophy of larval liver and hepatocytes (Fig. 11e and f). The presence of LEN in cell culture medium also significantly prevented the enlargement of FD Huh7 cells (Fig. 11g). These results suggested the involvement of TNF α activity in FD-induced hepatomegaly. This viewpoint was further supported by the increased expression of mmp13a, one

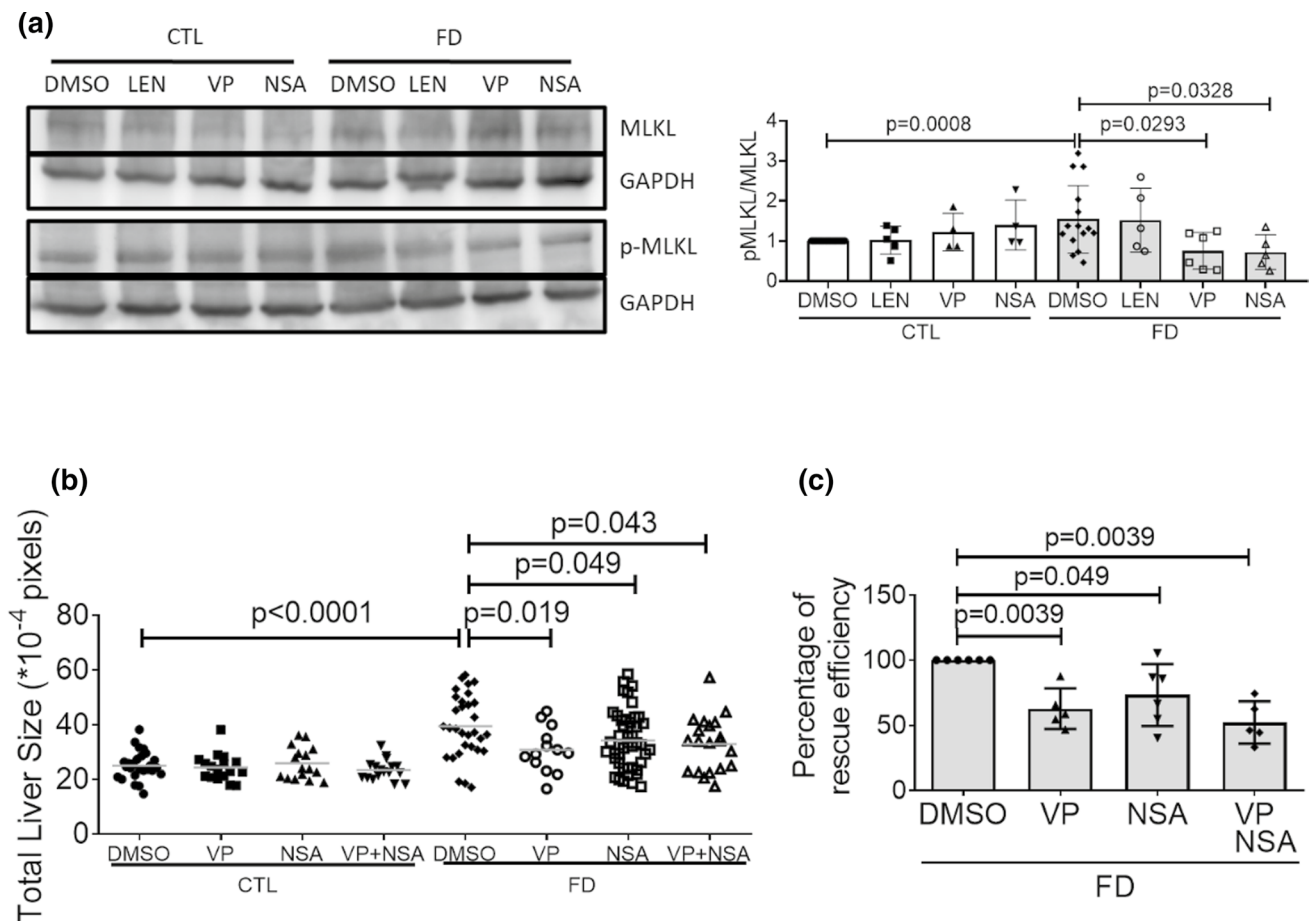


Fig. 9 The lack of additive rescuing effects upon co-exposure to verteporfin and NSA for FD-induced hepatomegaly. **a** The cell lysates prepared from Huh7 cells cultivated in FD medium in the presence of LEN (TNF α inhibitor, 4 μ M), VP (Hippo pathway inhibitor, 0.1 μ M) or NSA (necroptosis inhibitor, 2 μ M) for 8 days were analyzed with Western blotting for MLKL phosphorylation and quantified. **b** Larvae were exposed to VP (0.62 μ M) and NSA (5 μ M) either separately or simultaneously from 7 to 11 dpf. Larvae were imaged at 11 dpf and larval liver size was quantified with on-line software Image J. **c**

VP (0.1 μ M) and NSA (2 μ M) were added to FD cultured medium for Huh7 cells separately or simultaneously 5-day post-seeding. Cell sizes were measured on 8 dps with flow cytometry and calculated for the percentage of rescuing efficiency. Shown here are the averaged results of at least three independent trials. *LEN* lenalidomide, *VP* verteporfin, *NSA* necrosulfonamide. Statistical results are represented in the mean \pm SEM. *CTL* control (Tg-GGH/LR larvae without FD or Huh7 cells cultured in regular α -MEM), *FD* folate deficiency

of the metalloproteases responsible for TNF α cleavage and activation, in FD larval liver (Fig. 11h). Adding CL-82198, an MMP13 inhibitor, has successfully prevented FD-induced hepatomegaly (Fig. 11i). On the other hand, no significant difference in the expression level of adam17b, the other major metalloprotease mediating TNF α activation in extracellular matrix, was observed, suggesting that Adam17 did not contribute significantly to the activation of TNF α in FD larvae. Our results showed that FD-induced increase of TNF α activity was tissue-specific and partly due to the increased mmp13a expression. Meanwhile, the increased TNF α contributed to Hippo/YAP pathway activation and likely the subsequent hepatomegaly.

Discussion

We reported in the current studies that it is the interplay among the multiple pathways operating both in parallel and interactively, instead of merely the disturbed nucleotide supply, plays the decisive role in FD-induced hepatocytes enlargement. With the model of the transgenic FD zebrafish, which displays inducible folate deficiency and enlarged liver, we found that increased liver cell size is the major cause for the FD-induced hepatomegaly. Based on our results and the information reported in the literature [41–43], a prospective pathomechanism contributing to the FD-induced hepatocytes enlargement has been depicted

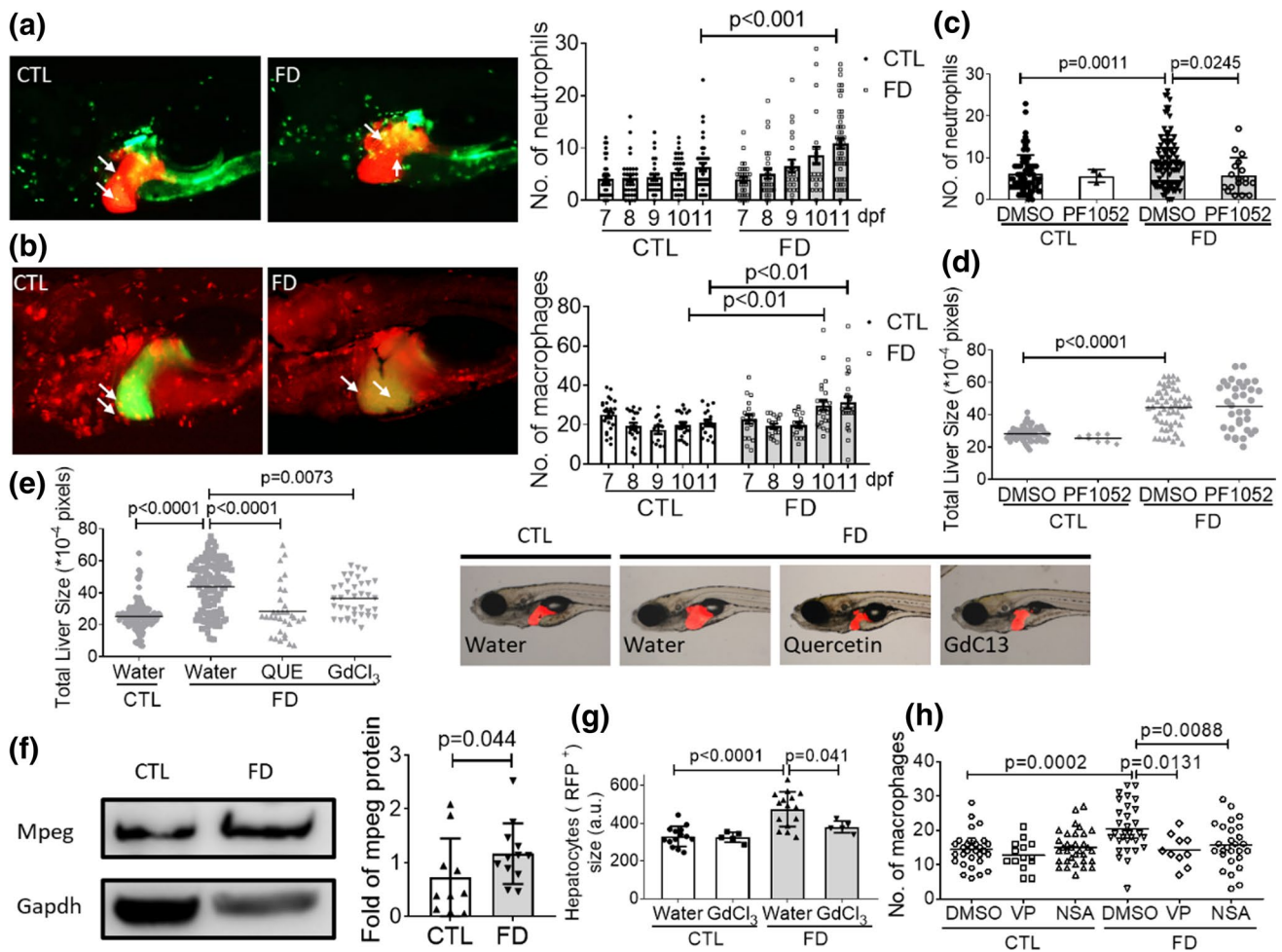


Fig. 10 Inflammatory cells infiltration was observed in FD larval liver. The FD larvae, generated from *Tg(lfabp:mCherry/hsp70:eGFP-γGH/mpx:eGFP)* (a) and *Tg(lfabp:eGFP/hsp70:mCherry-γGH/mpeg1:mCherry)* (b), were imaged at 11 dpf. The number of neutrophil (green fluorescent dots in a) and macrophages (red fluorescent dots in (b)) was counted and recorded daily. Data were collected from at least three independent trials with total larvae number ranging from 23 to 57 for each group. The number of neutrophils in liver area (c) and liver size (d) of larvae exposed to PF1052 (0.1625 μM) starting from 7 dpf was examined at 11 dpf as described before. e The liver sizes of larvae exposed to macrophage inhibitors, quercetin (QUE, 2.5 μM) and GdCl₃ (20 μM), were imaged and quantified at 11 dpf. Presented here are the averages of at least three independent trials with the total larval number of 24–47 for each group. f The

liver extracts prepared from FD adult fish were subjected to Western blotting with anti-mpeg antibodies. The signal intensity of Mpeg was quantified with densitometry. g FACS analysis on the sizes of hepatocytes isolated from FD larvae revealed significant improvement for those in the group treated with GdCl₃. The cell size obtained with flow cytometry (FSC) was reported in arbitrary units (a.u.). h Larvae were exposed to VP (Hippo pathway inhibitor, 0.62 μM) and NSA (necroptosis inhibitor, 5 μM) starting from 7 dpf and counted for the number of macrophages in larval liver area. Shown here are the averaged results of at least five independent trials with each sample prepared from 20 to 30 larvae. Statistical results are represented in the mean ± SEM. CTL control (larvae or adult fish without FD), FD folate deficiency

(Fig. 12): FD triggered necroptosis and Hippo/YAP pathway, leading to enlarged hepatocyte and hepatomegaly. FD also caused inflammation and macrophages infiltration in liver, which acts as an additional route to activate necroptotic pathway and YAP signaling via the increased TNFα and MMP13. MMP13 is a metalloprotease most abundant in extracellular environment and mediates TNFα cleavage and activation. In addition, FD-induced inflammation and necroptosis would convene a dialog of positive feedback loops, further deteriorating hepatomegaly. Hippo

signaling is one of the best-known pathways that controls organ size and involves in multifarious hepatic pathogenesis when dysregulated [36, 44]. No dedicated receptor on cell membrane has hitherto been identified for the activation of Hippo pathway. Instead, several physiological cues and cellular processes, including inflammation, biochemical signals and molecules from other pathway, have been shown to trigger YAP transcriptional network. Hippo pathway may also respond to physical milieu, such as tissue architecture including cell density, tissue tension

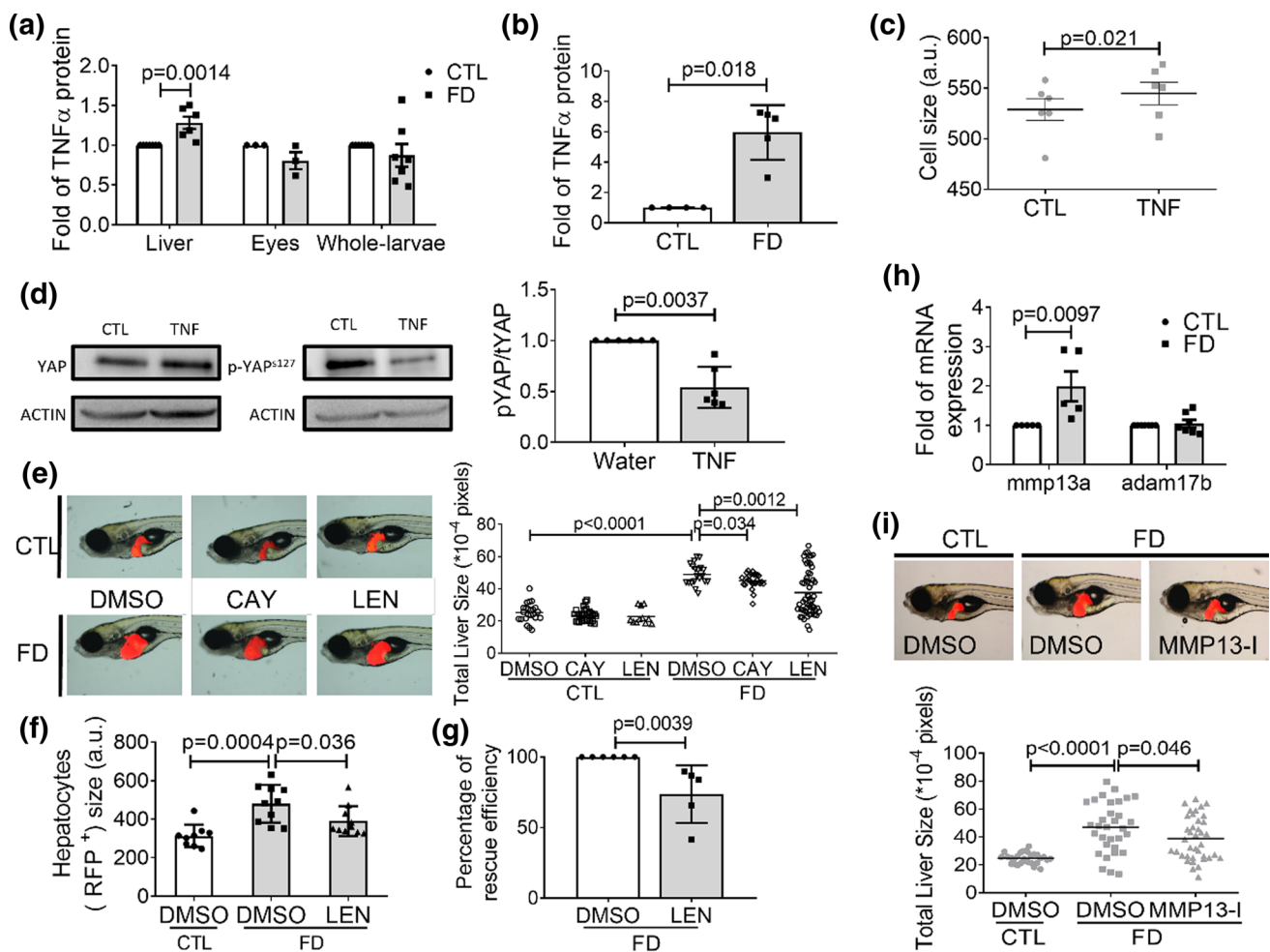


Fig. 11 TNF α contributed to Hippo/Yap pathway activation and FD-induced hepatomegaly. The tissue homogenate prepared from larvae at 11 dpf (a) and the used FD medium after cultivating Huh7 cells for 8 days (b) were quantified for TNF α protein level with ELISA. Huh7 cells cultivated in regular α -MEM with/without the exogenously added TNF α protein for 48 h were examined for cell size with flow cytometry (c) and analyzed for YAP expression and phosphorylation (d). The liver sizes of the larvae incubated in embryo water containing TNF α inhibitor LEN (38.5 μ M) or CAY10500 (1 μ M) starting from 7 dpf were imaged and quantified at 11 dpf under a fluorescence dissecting microscope (e). f The livers isolated from the larvae of 11 dpf were dispersed and the hepatocytes were examined for cell size with FACS. Shown here are the averaged results of at least four independent trials with each sample prepared from 20 to 30 larvae.

g LEN (TNF α inhibitor, 4 μ M) was added to FD cultured medium for Huh7 cells 5-day post-seeding. Cell sizes were measured on 8 dpf with flow cytometry and calculated for the percentage of rescuing efficiency. h The expression of *mmp13a* and *adam17b* in the liver isolated from FD larvae at 11 dpf were quantified with real-time PCR. i The liver size of larvae exposed to MMP13 inhibitor was quantified at 11 dpf. The continuous presence of MMP13 inhibitor in embryo water upon FD induction significantly alleviated liver hypertrophy. All the data presented above are the averages of at least three independent trials. The cell size obtained with flow cytometry (FSC) was reported in arbitrary units (a.u.). Statistical results are represented in the mean \pm SEM. CTL control (cells or larvae without FD), FD folate deficiency, LEN lenalidomide, MMP13-I MMP13 inhibitor

and shear stress [45]. Our findings unveiled a novel avenue through which the activity of Hippo pathway is modulated and the impact of folate status to cell size control is executed. These results substantiate the interplay among intracellular folate status, pathways regulation, inflammatory responses, actin cytoskeleton and cell volume control, which occurs in liver and can be best observed only with in vivo platform. Our findings also provide the evidence for an additional patho-mechanism contributing to hepatomegaly from the prospect of micronutrient, which may be

taken into consideration in future development of prophylactic and therapeutic strategies for liver diseases.

Our data suggested that the enlargement of hepatocytes in response to FD is largely due to the interplay among the multiple pathways, including inflammatory response, instead of disturbed nucleotide supply. The findings that supplementing FD larvae with dNTP failed to prevent hepatomegaly are unexpected. This is because megaloblastic anemia, a hall-mark clinical manifestation of FD with the characteristics of enlarged red blood cells, is reversible

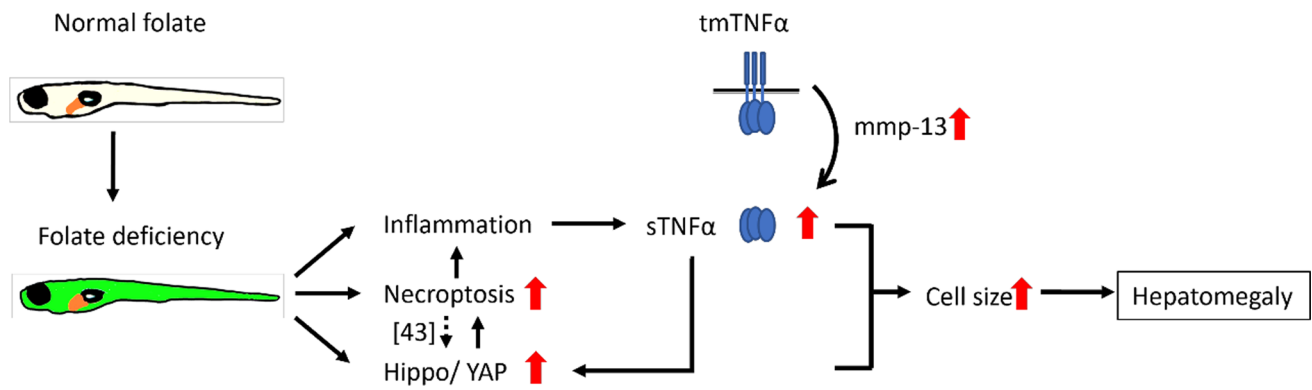


Fig. 12 The prospective pathomechanism contributing to the FD-induced hepatomegaly. FD triggers necroptosis and Hippo/YAP pathway, leading to enlarged hepatocyte and hepatomegaly. FD also caused inflammation and macrophages infiltration in liver, which act as an additional route to activate necroptotic pathway and YAP sign-

aling via increasing TNF α activity and mmp13, the metalloprotease mediating TNF α cleavage and activation. The FD-induced inflammation and necroptosis convene a dialog of positive feedback loops, further deteriorating hepatomegaly

with exogenous provision of nucleotides, suggesting a major role for nucleotide depletion and impaired DNA synthesis in the disease etiology [46]. These unexpected results could be readily explained by two observations. First, no significant cell proliferation and liver growth in the control larvae at the stages of 6–11 dpf. In addition, the intracellular 10-formyl-THF level in developing larvae is stably maintained even in FD larvae (Fig. 3f). 10-formyl-THF is the source of the formyl group for the C2 and C8 of purine in de novo synthesis. A constant level of 10-formyl-THF shall ensure a stable supply for nucleotides. This speculation is further supported by the subsequent findings that 10-CHO-THF concentrations remained constant always; whereas THF and 5-CH₃-THF levels changed along with the fluctuating folate status. Studies showed that modulating the expression of folate enzymes in OCM, especially those responsible for generating 10-formyl-THF, would allow the embryos to prioritize nucleotide supply in response to FD [47]. Our results also affirm the current viewpoint that the nucleotides formation was maintained in the expense of other biochemical reactions such as 5-CH₃-THF for SAM formation. Our data convey a possibility that FD may execute its effects through a non-canonical activity since increasing evidence also suggested that folate and folate metabolic enzymes possess non-metabolic functions in cell signaling and cancer biology [48]. That whether and how altered intracellular folate content ignites these non-metabolic signaling pathways modulating cell volume merits further investigation.

Different cell type/tissue appears to respond differentially to FD and supplementary rescuing agents. This is likely a reflection of tissue/cell type specificity of folate-mediated OCM. FOCM cell type/tissue specificity includes the variation in the regulatory mechanisms of OCM, as well as the cellular/tissue response to altered folate status. We found that cell enlargement occurred to Huh7 cells and 293 T cells,

but not SK-N-SH cells, although polyploid cells accumulation was observed in all three cell lines. Polyploidization is a potential factor causing cell enlargement and is beneficial to cells by increasing cell fitness without disrupting cell and tissue structure and to improve cell tolerance to genomic stress and apoptotic signals [49]. SK-N-SH cells also displayed polyploid cell accumulation, but did not show increased cell size correspondingly. These observations suggest that factors other than cell ploidy may also contribute to cell size control in response to FD. We also noticed the differential accumulation of FD cells at different cell cycle stages for different cell types. The increase at S-phase for Huh7 cells and at G2/M phase for SK-N-SH cells indicates that different types of cells respond to FD differentially. The absence of consistency between the change in cell size and the alteration in cell cycle/polyploidy supports the cell type/tissue specificity of FOCM. Lack of obvious alteration in the distribution of cytoskeleton may contribute to the unaffected cell size observed for FD SK-N-SH cells, which will be further discussed below.

The FOCM cell type/tissue specificity is also presented in the variation of cellular/tissue responses to altered folate status. Studies showed that FD-induced anomalies responded multifariously to rescuing agents. Nucleotides supplementation failed to prevent FD-induced hepatomegaly, as shown in the current study, and the impaired cardiogenesis and obstructed visual development, but effectively rescued the enlarged red cells, impeded hematopoiesis and malformed eyes observed in FD larvae [47, 50]. By the same token, folic acid did not improve hematopoiesis and swim bladder development but successfully prevents the cardiac anomalies found in FD larvae [50, 51]. Some FD-induced phenotypes even got worse when folic acid was used for rescue. For example, the UVB-inflicted larval tail damage become more severe when folic acid was added to embryos [52].

This cell/tissue type-specific response may be attributed to the different folate content among tissues and the incoherent distribution of folate derivatives resulting from the differential regulation of folate-mediated OCM [47]. It also reflects the complexity and context-dependent control of folate metabolism for maintaining a tissue-specific one-carbon homeostasis, which empowers the cells/tissues to prioritize the essential biochemical pathways to fulfill the needs under a circumstance. There is also a possibility that the cell-type specificity resides in the different non-metabolic signaling pathways triggered by FD, which guards the cell volume and varies among different types of cells. To be aware of the phenomenon of FOCM tissue specificity shall be vital since this differential specificity will render the tissues different vulnerability to altered folate status (both folate deficiency and sufficiency), hence different demands (responses) for folate supplementation. We are convinced that the knowledge on FOCM tissue specificity is crucial for optimizing the use of folate supplementation and anti-folate drug for diseases prevention and treatment. Further investigation on how the cell type specificity is established shall provide valuable insight to the control of folate-mediated OCM and references for folate supplementation.

Circumferential re-allocation of intracellular F-actin at the edge under cell membrane was found in FD Huh7 cells, which likely contributed to the hepatocyte enlargement and elevated liver stiffness observed in FD zebrafish. Alteration in cell size has been shown to change cell stiffness and cell fate [30]. Cell size has been tightly correlated with cell growth, metabolism and functional activity. Change in cell size reflects disturbed cellular homeostasis, which brings in further impact to cellular function and activity. By sensing and mediating extracellular signals, such as inflammatory cytokine TNF α , as well as coordinating with ion channels activity, actin cytoskeleton is crucial in determining cell volume [53, 54]. Currently, the direct evidence connecting intracellular folate status to actin and cell/tissue stiffness are limited. However, studies have shown that modulating the expression of 10-formyltetrahydrofolate dehydrogenase (FDH, ALDH1L1), a cytosolic folate enzyme, disturbed actin dynamics both in vitro and in vivo [55, 56]. Knocking down FDH obstructed F-actin polymerization and delayed epiboly in zebrafish embryogenesis. FDH is most abundant in liver, comprising 1% of total soluble protein in the liver of mammals and zebrafish [56, 57]. This tetrameric enzyme converts 10-CHO-THF to THF and formate. It also binds to its own product THF tightly and serves as a reservoir to store and stabilize tetrahydrofolate. Therefore, it is conceivable that decreasing FDH level likely led to a decreased intracellular folate content of hepatocytes. Although the total folate contents in those two studies were not reported, knocking down FDH expression indeed lowered the intracellular tetrahydrofolate level of zebrafish larvae [56].

We noticed that the intracellular folate content of SK-N-SH cells was fivefold higher than those in Huh7 cells and 293 T cells, of liver and kidney origins, respectively. The higher content of intracellular folate may imply a greater need for folate for SK-N-SH cells and a different homeostatic regulation for folate-mediated OCM (i.e., the composition of intracellular folate derivatives and folate enzymes, in terms of species and content). On the other hand, it may also convey a different sensitivity of cells to FD. It is interesting to note that SK-N-SH cells, when cultivated in FD medium, displayed neither change in cell size nor apparent alteration in the distribution of microtubule and actin filament (data not shown). These results support our speculation that the circumferential re-allocation of intracellular F-actin at the edge under cell membrane in FD Huh7 cells might contribute to the hepatocyte enlargement and elevated liver stiffness observed in FD zebrafish, as well as echo the correlation between cytoskeleton distribution and cell size control. We are convinced that the cell/tissue-specific regulation for folate metabolism and homeostasis, in conjunction with actin dynamics control and cell size regulation, merit further investigation.

Both Nec-1 and GSK872 were tested in the current study for examining the participation of RIPK1 and RIPK3, respectively. Studies showed that RIPK3 is essential for the activation of necroptosis. On the other hand, RIPK1 may (RIPK1-dependent) or may not (RIPK1-independent) be required for intervening necroptosis. Evidence even suggested that depletion of RIPK1 activity facilitated necroptosis triggered by TNF [58]. We noticed that the presence of Nec-1, a RIPK1 inhibitor, ameliorated FD-induced hepatomegaly but did not prevent the enlargement of larval hepatocytes. These results suggest that the FD-induced hepatocytic enlargement is via a RIPK1-independent pathway. In another word, RIPK1 may affect liver size indirectly and passively. Our observations also imply a possibility that factor other than enlarged cell size, which is also sensitive to RIPK1 activity, may also contribute to the liver enlargement observed in FD larvae.

The results that multiple pathways contribute to liver enlargement found in FD zebrafish larvae reflect the complexity of the etiology for hepatomegaly. Hepatomegaly is the most common and earliest detectable sign of many liver diseases, including fatty liver diseases, alcoholic hepatitis, non-alcoholic fatty liver disease and hepatic tumors. As the disease progressing and passing the stage of hepatomegaly, the damage may become irreparable and ultimately lead to liver failure, cirrhosis, cancer and even death. Hepatomegaly is also a non-specific pathological sign of multifarious causes, such as obesity, infection, metabolic syndrome, autoimmune disease and toxification. Although the etiology of hepatomegaly is diverse, the resulting pathological hypertrophy may cause a similar progression of disease

and hinder the effect of subsequent treatment. Currently, the patho-mechanism underlying hepatomegaly remain incompletely understood and is considered multifarious. The results reported in the current studies, as well as the zebrafish transgenic line displaying FD-induced hepatomegaly, may provide reference for developing both prophylactic and therapeutic strategies for the early treatment of liver disease.

Author contributions T-FF conceptualized this study and responsible for funding acquisition. W-YC, T-HH, G-HL, and I-HS performed the experiments. W-YC and T-FF designed the experiments, analyzed the data, and wrote the manuscript. B-HC and M-JT reviewed and provided consultancy for experimental design and data analysis. All authors contributed to the article and approved the submitted version.

Funding This work was supported by the research grants (MOST 106-2311-B-006-004-MY3; MOST 109-2320-B-006-051) to TFF. We are also grateful for the material support from Taiwan Zebrafish Core Facility (support by MOST 104-2321-B-001-045), the technical support from the Core Research Laboratory, College of Medicine, National Cheng Kung University.

Data availability Enquiries about data availability should be directed to the authors.

Declarations

Conflict of interest The authors have declared that no conflict of interest exists.

Ethical approval All usage and experiments of adult and embryo were approved by the Institutional Animal Care and Use Committee, National Cheng Kung University, Tainan, Taiwan (IACUC Approval No. 106086).

Consent to participate No consent to participate was required in the completion of this article.

Consent for publication All authors consent to publication.

References

- van de Pol ILE, Flik G, Verberk W (2020) Triploidy in zebrafish larvae: Effects on gene expression, cell size and cell number, growth, development and swimming performance. *PLoS ONE* 15(3):e0229468. <https://doi.org/10.1371/journal.pone.0229468>
- Miettinen TP et al (2014) Identification of transcriptional and metabolic programs related to mammalian cell size. *Curr Biol* 24(6):598–608. <https://doi.org/10.1016/j.cub.2014.01.071>
- Marguerat S et al (2012) Quantitative analysis of fission yeast transcriptomes and proteomes in proliferating and quiescent cells. *Cell* 151(3):671–683. <https://doi.org/10.1016/j.cell.2012.09.019>
- Velayutham N, Agnew EJ, Yutzey KE (2019) Postnatal cardiac development and regenerative potential in large mammals. *Pediatr Cardiol* 40(7):1345–1358. <https://doi.org/10.1007/s00246-019-02163-7>
- Habib SL (2014) Tuberin in renal cell hypertrophy. *Cell Cycle* 13(6):869–870. <https://doi.org/10.4161/cc.27942>
- Marshall WF et al (2012) What determines cell size? *BMC Biol* 10:101. <https://doi.org/10.1186/1741-7007-10-101>
- Cox AG et al (2016) Yap reprograms glutamine metabolism to increase nucleotide biosynthesis and enable liver growth. *Nat Cell Biol* 18(8):886–896. <https://doi.org/10.1038/ncb3389>
- Miettinen TP, Björklund M (2015) Mevalonate pathway regulates cell size homeostasis and proteostasis through autophagy. *Cell Rep* 13(11):2610–2620. <https://doi.org/10.1016/j.celrep.2015.11.045>
- Yamamoto K et al (2014) Largen: a molecular regulator of mammalian cell size control. *Mol Cell* 53(6):904–915. <https://doi.org/10.1016/j.molcel.2014.02.028>
- Pérez-Hidalgo L, Moreno S (2016) Nutrients control cell size. *Cell Cycle* 15(13):1655–1656. <https://doi.org/10.1080/15384101.2016.1172471>
- Yao Z et al (2012) Regulation of cell size in response to nutrient availability by fatty acid biosynthesis in *Escherichia coli*. *Proc Natl Acad Sci U S A* 109(38):E2561–E2568. <https://doi.org/10.1073/pnas.1209742109>
- Kao TT et al (2014) Folate deficiency-induced oxidative stress contributes to neuropathy in young and aged zebrafish—implication in neural tube defects and Alzheimer’s diseases. *Neurobiol Dis* 71:234–244. <https://doi.org/10.1016/j.nbd.2014.08.004>
- Fox JT, Stover PJ (2008) Folate-mediated one-carbon metabolism. *Vitam Horm* 79:1–44. [https://doi.org/10.1016/s0083-6729\(08\)00401-9](https://doi.org/10.1016/s0083-6729(08)00401-9)
- Gliszczynska-Świgło A (2007) Folates as antioxidants. *Food Chem* 101(4):1480–1483
- Fan J et al (2014) Quantitative flux analysis reveals folate-dependent NADPH production. *Nature* 510(7504):298–302. <https://doi.org/10.1038/nature13236>
- Bailey LB et al (2015) Biomarkers of nutrition for development—folate review. *J Nutr* 145(7):1636s–1680s. <https://doi.org/10.3945/jn.114.206599>
- Czeizel AE et al (2013) Folate deficiency and folic acid supplementation: the prevention of neural-tube defects and congenital heart defects. *Nutrients* 5(11):4760–4775. <https://doi.org/10.3390/nu5114760>
- Zhang X et al (2021) The association between folate and Alzheimer’s disease: a systematic review and meta-analysis. *Front Neurosci* 15:661198. <https://doi.org/10.3389/fnins.2021.661198>
- Veinotte CJ, Dellaire G, Berman JN (2014) Hooking the big one: the potential of zebrafish xenotransplantation to reform cancer drug screening in the genomic era. *Dis Model Mech* 7(7):745–754. <https://doi.org/10.1242/dmm.015784>
- Klems A et al (2020) The GEF Trio controls endothelial cell size and arterial remodeling downstream of Vegf signaling in both zebrafish and cell models. *Nat Commun* 11(1):5319. <https://doi.org/10.1038/s41467-020-19008-0>
- Liu A, Ulrich C (2009) Genetic variability in folate-mediated one-carbon metabolism and risk of colorectal neoplasia. In: Potter J, Lindor N (eds) *Genetics of colorectal cancer*. Springer, New York, pp 223–242
- Westerfield M (2000) *The zebrafish book. A guide for the laboratory use of zebrafish (Danio rerio)*
- Fillatre J et al (2019) TEADs, Yap, Taz, Vgll4s transcription factors control the establishment of Left-Right asymmetry in zebrafish. *Elife*. <https://doi.org/10.7554/eLife.45241>
- Wang X et al (2014) Inhibitors of neutrophil recruitment identified using transgenic zebrafish to screen a natural product library. *Dis Model Mech* 7(1):163–169. <https://doi.org/10.1242/dmm.012047>
- Tsarouchas TM et al (2018) Dynamic control of proinflammatory cytokines Il-1 β and Tnf- α by macrophages in zebrafish spinal cord regeneration. *Nat Commun* 9(1):4670. <https://doi.org/10.1038/s41467-018-07036-w>

26. Kao TT et al (2013) Methotrexate-induced decrease in embryonic 5-methyl-tetrahydrofolate is irreversible with leucovorin supplementation. *Zebrafish*. <https://doi.org/10.1089/zeb.2013.0876>
27. Kao TT et al (2013) Methotrexate-induced decrease in embryonic 5-methyl-tetrahydrofolate is irreversible with leucovorin supplementation. *Zebrafish* 10(3):326–337. <https://doi.org/10.1089/zeb.2013.0876>
28. Huang A et al (2021) Inflammation-induced macrophage lysyl oxidase in adipose stiffening and dysfunction in obesity. *Clin Transl Med* 11(9):e543. <https://doi.org/10.1002/ctm2.543>
29. Chang WN, Lin HC, Fu TF (2010) Zebrafish 10-formyltetrahydrofolate dehydrogenase is similar to its mammalian isozymes for its structural and catalytic properties. *Protein Expr Purif* 72(2):217–222. <https://doi.org/10.1016/j.pep.2010.04.003>
30. Guo M et al (2017) Cell volume change through water efflux impacts cell stiffness and stem cell fate. *Proc Natl Acad Sci U S A* 114(41):E8618–E8627. <https://doi.org/10.1073/pnas.1705179114>
31. Nakabayashi H et al (1982) Growth of human hepatoma cells lines with differentiated functions in chemically defined medium. *Cancer Res* 42(9):3858–3863
32. Pear WS et al (1993) Production of high-titer helper-free retroviruses by transient transfection. *Proc Natl Acad Sci U S A* 90(18):8392–8396. <https://doi.org/10.1073/pnas.90.18.8392>
33. Biedler JL, Helson L, Spengler BA (1973) Morphology and growth, tumorigenicity, and cytogenetics of human neuroblastoma cells in continuous culture. *Cancer Res* 33(11):2643–2652
34. Molnar T et al (2019) Current translational potential and underlying molecular mechanisms of necroptosis. *Cell Death Dis* 10(11):860. <https://doi.org/10.1038/s41419-019-2094-z>
35. Chen D, Yu J, Zhang L (2016) Necroptosis: an alternative cell death program defending against cancer. *Biochim Biophys Acta* 1865(2):228–236. <https://doi.org/10.1016/j.bbcan.2016.03.003>
36. Werneburg N, Gores GJ, Smoot RL (2020) The hippo pathway and YAP signaling: emerging concepts in regulation, signaling, and experimental targeting strategies with implications for hepatobiliary malignancies. *Gene Expr* 20(1):67–74. <https://doi.org/10.37271/105221619X15617324583639>
37. Chen PY et al (2020) Increased leptin-b expression and metalloprotease expression contributed to the pyridoxine-associated toxicity in zebrafish larvae displaying seizure-like behavior. *Biochem Pharmacol* 182:114294. <https://doi.org/10.1016/j.bcp.2020.114294>
38. Wang S et al (2020) The crosstalk between hippo-YAP pathway and innate immunity. *Front Immunol* 11:323. <https://doi.org/10.3389/fimmu.2020.00323>
39. Zhou Y et al (2018) Emerging roles of hippo signaling in inflammation and YAP-driven tumor immunity. *Cancer Lett* 426:73–79. <https://doi.org/10.1016/j.canlet.2018.04.004>
40. Kolb AF, Petrie L (2013) Folate deficiency enhances the inflammatory response of macrophages. *Mol Immunol* 54(2):164–172. <https://doi.org/10.1016/j.molimm.2012.11.012>
41. Yang F et al (2019) TNF α -mediated necroptosis aggravates ischemia-reperfusion injury in the fatty liver by regulating the inflammatory response. *Oxid Med Cell Longev* 2019:2301903. <https://doi.org/10.1155/2019/2301903>
42. Chen AQ et al (2019) Microglia-derived TNF- α mediates endothelial necroptosis aggravating blood brain-barrier disruption after ischemic stroke. *Cell Death Dis* 10(7):487. <https://doi.org/10.1038/s41419-019-1716-9>
43. Lin CC et al (2020) RIPK3 upregulation confers robust proliferation and collateral cystine-dependence on breast cancer recurrence. *Cell Death Differ* 27(7):2234–2247. <https://doi.org/10.1038/s41418-020-0499-y>
44. Bou Saleh M et al (2021) Loss of hepatocyte identity following aberrant YAP activation: a key mechanism in alcoholic hepatitis. *J Hepatol* 75(4):912–923. <https://doi.org/10.1016/j.jhep.2021.05.041>
45. Dasgupta I, McCollum D (2019) Control of cellular responses to mechanical cues through YAP/TAZ regulation. *J Biol Chem* 294(46):17693–17706. <https://doi.org/10.1074/jbc.REV119.007963>
46. Koury MJ, Price JO, Hicks GG (2000) Apoptosis in megaloblastic anemia occurs during DNA synthesis by a p53-independent, nucleoside-reversible mechanism. *Blood* 96(9):3249–3255
47. Hsiao TH et al (2021) The incoherent fluctuation of folate pools and differential regulation of folate enzymes prioritize nucleotide supply in the zebrafish model displaying folate deficiency-induced microphthalmia and visual defects. *Front Cell Dev Biol* 9:702969. <https://doi.org/10.3389/fcell.2021.702969>
48. Shang M et al (2021) The folate cycle enzyme MTHFD2 induces cancer immune evasion through PD-L1 up-regulation. *Nat Commun* 12(1):1940. <https://doi.org/10.1038/s41467-021-22173-5>
49. Orr-Weaver TL (2015) When bigger is better: the role of polyploidy in organogenesis. *Trends Genet* 31(6):307–315. <https://doi.org/10.1016/j.tig.2015.03.011>
50. Tu HC et al (2017) One crisis, diverse impacts-tissue-specificity of folate deficiency-induced circulation defects in zebrafish larvae. *PLoS ONE* 12(11):e0188585. <https://doi.org/10.1371/journal.pone.0188585>
51. Lee GH et al (2019) A novel zebrafish model to emulate lung injury by folate deficiency-induced swim bladder defectiveness and protease/antiprotease expression imbalance. *Sci Rep* 9(1):12633. <https://doi.org/10.1038/s41598-019-49152-7>
52. Tu HC et al (2019) Supplementation with 5-formyltetrahydrofolate alleviates ultraviolet B-inflicted oxidative damage in folate-deficient zebrafish. *Ecotoxicol Environ Saf* 182:109380. <https://doi.org/10.1016/j.ecoenv.2019.109380>
53. Koukouritaki SB et al (1999) TNF- α induces actin cytoskeleton reorganization in glomerular epithelial cells involving tyrosine phosphorylation of paxillin and focal adhesion kinase. *Mol Med* 5(6):382–392
54. Papakonstanti EA, Vardaki EA, Stournaras C (2000) Actin cytoskeleton: a signaling sensor in cell volume regulation. *Cell Physiol Biochem* 10(5–6):257–264. <https://doi.org/10.1159/000016366>
55. Oleinik NV, Krupenko NI, Krupenko SA (2010) ALDH1L1 inhibits cell motility via dephosphorylation of cofilin by PP1 and PP2A. *Oncogene* 29(47):6233–6244. <https://doi.org/10.1038/onc.2010.356>
56. Chang WN et al (2014) Knocking down 10-Formyltetrahydrofolate dehydrogenase increased oxidative stress and impeded zebrafish embryogenesis by obstructing morphogenetic movement. *Biochim Biophys Acta* 1840(7):2340–2350. <https://doi.org/10.1016/j.bbagen.2014.04.009>
57. Schirch D et al (1994) Domain structure and function of 10-formyltetrahydrofolate dehydrogenase. *J Biol Chem* 269(40):24728–24735
58. Weinlich R et al (2017) Necroptosis in development, inflammation and disease. *Nat Rev Mol Cell Biol* 18(2):127–136. <https://doi.org/10.1038/nrm.2016.149>

Publisher's Note Springer Nature remains neutral with regard to jurisdictional claims in published maps and institutional affiliations.